

Republic of Iraq
Ministry of Higher Education
and Scientific Research
University of Kerbala



The Effect of Vibration on The Pressure Distribution of Journal Bearing

A Thesis

*Submitted to the College of Engineering / University of Kerbala in
Partial Fulfillment of Requirements for the Degree of Master of Science
in Mechanical Engineering*

(Applied Mechanics)

By

Huda Mseer Abdulkadum

(B.Sc.2014)

Supervised By

Asst. Prof. Dr. Abdulkareem Abdulrazzaq

2017 A.M

بِسْمِ اللَّهِ الرَّحْمَنِ الرَّحِيمِ

أَقْرَأْ بِاسْمِ رَبِّكَ الَّذِي خَلَقَ (١) خَلَقَ الْإِنْسَانَ مِنْ عَلَقٍ

(٢) أَقْرَأْ وَرَبُّكَ الْأَكْرَمُ (٣) الَّذِي عَلَّمَ بِالْقَلَمِ (٤) عَلَّمَ

الْإِنْسَانَ مَا لَمْ يَعْلَمْ (٥)

صدق الله العلي العظيم

سورة العلق (الآيات ١-٥)

SUPERVISOR CERTIFICATE

I certify that this thesis entitled "**The Effect of Vibration on The Pressure Distribution of Journal Bearing**" was prepared under my supervision at the Mechanical Engineering Department, University of Kerbala, as a partial fulfillment of the requirements for the degree of Master of Science in Mechanical Engineering.

Signature

Asst. Prof. Dr. Abdulkareem Abdulrazzaq Alhumdany

(Supervisor)

Data / /

ACNOWLEDGMENT

(In The Name of Allah, The Gracious, The Merciful)

First, of all I thank Allah who helped me in carrying out this thesis.

I wish to express my deep gratitude to my supervisor Dr. Abdulkareem Abdulrazzaq for his invaluable help, advice and encouragement during the various stages of the present work.

A great gratitude and thanks to my parents for supporting me during that period.

I record sincere gratitude to the head of Mechanical Engineering Department Dr. Hazem Omran for his effort. A great thanks to my Asst. lecture Murtada Shubar and to all those who have helped me throughout this research even by one word.

Finally, I would like to thank the staff of the laboratories of Mechanical Engineering Department for their great cooperation

Huda

2017

ABSTRACT

The journal bearing is considered an important part of most rotary machines. It is used to support the radial loads. It is necessary to prevent metal to metal contact between the stationary part (bearing) and the rotating part (shaft). It suffers unwanted oil whirl due to the high self-vibration and a cyclic loads and this causes the bearing instability.

In this thesis, the performance of the journal bearing at the steady state and dynamic loading condition under the effect of self-excitation and forced harmonic excitation has been investigated.

For this purpose, the hydrodynamic of a plain cylindrical journal bearing system has been adopted.

The conventional form of the Reynolds equation is analyzed analytically and numerically using the central finite difference technique with a proper initial and boundary condition.

The analysis has been achieved for the short journal bearing approximation.

The numerical equations then have been intended and written in the computer program (FORTRAN-95) to obtain the results.

The validity of the journal bearing device in the mechanical engineering laboratory in the university of Kerbala has been tested to study the pressure distribution of the journal bearing. The results obtained were compared with those of numerical and found to be of high discrepancy. So the experimental technique is excluded to be compared with the dynamic loading results.

According to the numerical results obtained, the maximum oil pressure was obtained under the combine effect of forced harmonic vibration and self- excitation is (14.8778 MPa) which is increased by 36.66 percent from those obtained under the self- excitation only. This value was

clearly increasing as the amplitude of vibration increases causing very high fluctuation which leads to failure.

It is found that the maximum value of lubricant pressure and the minimum film thickness under the effect of forced harmonic excitation was affected clearly by the frequency and damping ratios.

Where for the frequency ratio ($\omega/\omega_n < 1$), it is found that, the maximum pressure increased causes decreases in the minimum film thickness. While The maximum film pressure decreases for ($\omega/\omega_n > 1$), making the minimum film thickness to be increased preventing the metal to metal contact.

It is also found that, the higher damping ratio causes decreases in the amplitude of vibration and this lead to decreases the maximum film pressure and therefore increasing in the oil film thickness. For damping ratio higher than 0.5, there is a little effect on the minimum film thickness.

It is noticed that, the maximum oil film pressure is higher under the effect of harmonic external forced vibration only than for both self-excitation vibration and under the combined effect by (51.92, 24.1) percent respectively for the same specifications for journal and the oil. However, the maximum oil film pressure dose not reach to the value of heavily loaded journal bearing (2GPa.) to take the elastohydrodynamics effect into the consideration.

LIST OF CONTENTS

Abstract	I
List of contents	III
Nomenclature	V
List of tables	VII
List of figures	VIII
Chapter One – Introduction	1
1.1 General	1
1.2 The Objective of the present work	3
Chapter Two – Literature Review	4
2.1 Introduction	4
2.2 Literature review	4
Chapter Three – Mathematical Modeling	9
3.1 Geometry of journal bearing	9
3.2 Coordinates system	11
3.3 Reynold's equation	12
3.4 Steady state analysis	12
3.5. Dynamic condition	14
3.5.1 Self excitation	14
3.5.2 Forced harmonic excitation	15
3.6 Load Carrying Capacity	17
3.6.1 Load Carrying Capacity of Steady state	17

3.6.2 Load Carrying Capacity of Dynamic Condition	18
3.7 Numerical analysis	19
3.7.1 Mesh generation	20
3.7.2 Solving the Reynold's Equation	21
3.7.3 Solution procedure of steady state	22
3.7.4 Solution procedure of combine effect of the self-exited and forced harmonic vibration	23
3.8 Computer program	24
 Chapter Four – Experiment study	 30
4.1 Technical Description	30
4.2 Journal Bearing Set-up	30
4.3 Measurement elements	37
4.4 Loading system	39
4.5 Driving system	41
4.6 Lubricant system	43
 Chapter Five – Result and discussion	 44
5.1 Experimental results	46
5.2 Numerical results	49
5.2.1 Convergence steady	49
5.2.2 Steady state results	50
5.2.3 Dynamically loaded results	56
 Chapter Six – Conclusions and Recommendations	 75
6.1 Conclusions	75
6.2 Recommendations for future work	76
 References	 77

Appendices		79
Appendix-A	Derivation the stiffens of the shaft	79
Appendix-B	The Calibration of Instruments used in Thesis	81

NOMENCLATURE

The following symbols are used in the purview.

Symbol	Description	Units
c	Bearing radial clearance	m
D	Diameter of journal	m
e	Eccentricity of journal	m
E	The modules elasticity of the shaft	N/m ²
f	Amplitude of the vibration force	N
h	Oil film thickness	m
h_{max}	Maximum oil film thickness	m
h_{min}	Minimum oil film thickness	m
\bar{h}	Dimensionless oil film thickness (h/c)	
I	The geometrical moment of inertia	m ⁴
i, j	The indexes increase a long x, z axes	
K	Stiffness of the journal (shaft)	N/m
L	Bearing length	m
M	Mass of the journal (shaft)	Kg
N	Journal speed	rpm
P	Oil film pressure	Pa
\bar{P}	Dimensionless oil pressure $\bar{P} = \frac{p}{6\mu\omega} \left(\frac{c}{R}\right)^2$	
R	Journal radius	m
t	Total time	sec
u	Shaft speed	m/sec

W	Bearing load carrying capacity	N
W_0	Amplitude of load carrying capacity	N
x, y, z	Coordinate system	
\bar{x} . \bar{y} . \bar{z}	Dimensionless coordinate system	

Greek symbols

Symbol	Description	Units
ε	Eccentricity Ratio	-
ξ	Damping factor	-
μ	Lubrication viscosity	pa. s
ρ	Density of oil	Kg/m ³
φ	Bearing attitude angle	rad
ψ	Phase angle of oscillation	rad
ω	Journal rotational speed	rad/sec
ω_n	Journal Natural frequency	rad/sec

Superscript

-	Dimensionless quantity
---	------------------------

List of Tables

Tables	Title	Page
5-1	The journal bearing characteristic of experimental test.	44
5-2	The journal bearing characteristic of the case study	45
5-3	The expermental results	47
5-4	Convergence criteria	49
5-5	Maximum oil film pressure for different values of damping	69
5-6	Maximum oil film pressure distribution for different values (ω/ω_n)	71

List of Figure

Figures	Title	Page
3-1	Geometry of Journal Bearing	10
3-2	Oil film thickness and coordinate of the system of journal bearing	11
3.3	Discretization of oil film domain	20
3.4	Flowchart of program for steady state	25
3.5	Flowchart of program for dynamic condition	27
4-1	Journal bearing apparatus	31
4-2	The bearing bush	32
4-3	Schematic of the shaft	33
4-4	The journal (shaft).	34
4-5	Schematic of housing	35
4-6	The housing	35
4-7	The brackets	36
4-8	The coupling	36
4-9	The manometer device	37
4-10	Thermocouples type K	38
4-11	Pneumatic jig	39
4-12	Electrical compressor	39
4-13	Pressure gauge	40
4-14	Solenoid valve	40
4-15	3-phase motor	41
4-16	Speed recorder	41
4-17	Safety conductor	42
4-18	oil reservoir	43
5-1	The oil film Pressure obtained from the experimental	47

	test	
5-2	Numerical oil film pressure distribution of different value of eccentricity ratios up to 0.07	48
5-3	Numerical oil film pressure distribution of different value of eccentricity ratios up to 0.7	48
5-4	Oil film Pressure distribution at different values of eccentricity ratio	50
5-5	Oil film thickness at different values of eccentricity ratio	51
5-6	Maximum oil film pressure versus eccentricity ratio for different values of rotational speed	52
5-7	Oil film Pressure at different values of aspect ratio	53
5-8	Load carrying capacity versus eccentricity ratio.	53
5-9	Load carrying capacity versus rotational speed for different value of aspect ratios.	54
5-10	3-D Oil film pressure distribution along the circumferential direction of journal bearing	55
5-11	3-D Oil film thickness distribution along the circumferential direction of journal bearing	55
5-12	The velocity of the center of journal versus the non-dimensional response time for different value of φ under a sinusoidal load	56
5-13	The velocity of the center of journal versus the non-dimensional response time for different values of ε under a sinusoidal load	57
5-14	Oil film Pressure versus the circumferential direction for a different values of ε	68
5-15	Oil film Pressure distribution along the circumferential	59

	direction for a different value of φ	
5-16	Load carrying capacity versus eccentricity ratio for different values of rotational speeds.	59
5-17	Oil film Pressure distribution along the circumferential direction of journal bearing in 3-dimension.	60
5-18	Oil film Pressure at different value of amplitude of forced vibration	61
5-19	Maximum oil film pressure versus time for different values of damping ratio	62
5-20	Minimum film thickness verse damping ratio for different values of (ω/ω_n) .	63
5-21	Oil film pressure distribution for different values (ω/ω_n)	64
5-22	Oil film Pressure distribution along the circumferential direction of journal bearing in 3-dimension.	64
5-23	Maximum pressure distribution of the journal bearing with and without forced vibration effect during 1 sec	65
5-24	Oil film Pressure for different values of amplitude of forced vibration	66
5-25	Maximum pressure distribution versus damping ratio for different values of (ω/ω_n) .	67
5-26	Maximum oil film pressure for different values of damping ratio during 1 sec.	68
5-27	Maximum oil film pressure distribution for different values (ω/ω_n) during 1 sec	70
5-28	Maximum oil film pressure and minimum film	72

	thickness variation during 1 sec	
5-29	Minimum film thickness versus damping ratio for different values of (ω/ω_n) .	73
5-30	Oil film Pressure distribution along the circumferential direction of journal bearing in 3-dimension.	74

INTRODUCTION

1.1 General

Hydrodynamic bearings are utilized to support rotating shafts of heavy machines. The fluid film bearing and rolling element bearing are the two common sorts of bearings which are generally utilized as a part of rotor-bearing system applications. The fluid film bearings are utilized as a part of bunch of substantial numbers of applications, from small electric engines, to vehicle and airplane cylinder motors, to large steam turbines for electric power generation [1].

The hydrodynamic fluid film created plays an essential part in the stability, because of its damping qualities [2].

The main type of hydrodynamic bearing is the journal bearing. It consists of circular sleeve (bearing or bushing) around a rotating shaft with diameter larger than that of a journal (shaft). A journal bearing supports a radial load. If the bearing extends around the full 360° of the journal, it is called a full journal bearing. If a wrap angle is less than 360°, it is called a partial journal bearing.

Journal bearings are designed in such a way to reduce friction and to minimize wear and rupture risks, so that even in the worst conditions, journal and bearing are not expected to come in contact [2].

Journal bearings have a self-excited instability, which is generally called the self-excited oil whirl. The reason for the instability is due to the imbalance-induced vibration.

Vibration caused by mass imbalance, which is known as the self-excited vibration, is a significant factor restricting the performance and fatigue life of a rotating system [3].

External vibrations, the other source of instability, can seriously threaten the safety and working performance of rotating machinery. The risk severity is generally dependent upon the response level of inner machine parts in respect to the level of the externally-applied vibrations.

The present work consists of two parts, theoretical and experimental to study the effect of external vibrations on the pressure distribution of journal bearing. The governing equation of Reynold coupled with vibrations equation are solved analytically and numerically by assuming the short bearing theory (Ockvirck approximation) to determine pressure distribution in the fluid film.

It is then integrated to obtain the load carrying capacity of short journal bearing.

For numerical calculations a finite difference method has been used with appropriate initial and boundary conditions. The central node technique is used in finite difference method. It is used for this purpose the computer program written by using (FORTRAN 95) to solve the governing equations.

1.2 Objectives of the present work

The main objective of this work summarized in the following steps:

- 1- Determine the pressure distribution of short journal bearing for steady state theoretically and experimentally.
- 2- Determine the pressure distribution of short journal bearing due to external harmonic excitation so the study include the pressure distribution under different values of $\left(\frac{\omega}{\omega_n}\right)$ and amplitude of harmonic excitation (F_o).

LITERATURES REVIEW

2.1 Introduction

The study of the vibration effect on the pressure distribution and the dynamic characteristics has been considered to be an important subject in the field of tribology.

In the following, a review of literature relating the effect of vibration due to mass unbalance of the shaft (journal) and a self-excited instability which affects on the performance of bearings.

2.2 Literatures review

Uğur YÜCEL, [1], Solved the Reynolds equation analytically for computing the stiffness and damping coefficients of journal bearings by using short bearing approximation.

These coefficients obtained by integration pressure which defines the forces of bearing and the corresponding dynamic characteristics of short journal bearing.

The dynamic coefficients are very important for dynamic calculations of unbalanced response, damped natural frequencies, and stability analysis.

Paulo Flores, et. al, [2], presented an accurate, reality and simple graphical strategy named the analytical mobility technique to analyze and solve the equations of finite journal bearing subjected to variable dynamic load. The mobility method is a graphical method it used to find the journal center orbit marching in time from initial eccentricity ratio.

The researcher showed that this technique is computationally efficient because the equation of journal bearing motion are written in such a way

avoiding the need for time consuming as in the conventional solution of Reynolds equation so this method is very fast.

They considered both short and long bearing assumption and gave an analytic solution for short bearing approximation.

They found that the maximum pressure in short bearing theory is 6.5 MPa

A. Bouzidane, M. Thomas, [3], studied the dynamic behavior of a rotor supported by a hydrostatic journal bearing. They used a Newtonian fluid as a lubricant with a viscosity which decreases when an electric field is applied and which can restore its property when the field is removed.

This fluid is named a negative electrorheological fluid (NER).

These fluids are suitable for the real time control of damping the vibration.

They used the central finite difference to solve the Reynolds equation.

They investigate the effect of NER, recess pressure and static eccentricity ratio on the load carrying capacity, flow, stiffness and damping.

The response of a damped system under a harmonic force is presented.

It is found that the electric field has no effect on the stiffness of hydrostatic bearing and decrease as a film thickness increases due to the increasing in eccentricity ratio.

Also they noticed that, the use of NER is not necessary because this fluid can be activated when operating at a speed higher than critical speed without increasing rotor vibration. Furthermore, the usage of a fluid with a high viscosity in order to obtain a high damping is preferred. So the vibratory response of the rotor excited by an unbalance can be reduced.

NB Naduvinamani et. al, [4], Considered the coupled stress fluid as the lubrication to study its rheological effects on the static and dynamic

behavior without journal rotation for porous journal bearing. The analysis was achieved in the case of a constant and cyclic loading.

The dynamic loading was analyzed by considering the variety in the velocity of the journal center.

They found that the journal center velocity decreases while the squeeze film pressure and load carrying capacity increases for coupled stress as compared with the Newtonian case.

The main result of this research is that to give the designer a data base to choose a reasonable values for the parameters in order to accomplish the optimum bearing performance

M. Senthil Kumar, et. al [5], gave a numerical solution by using finite difference method for Reynolds equation to obtain the static and dynamic oil film pressure for finite length journal bearing. They presented the proposed method for the pressure distribution, oil film thickness for static and dynamic conditions.

They showed that the steady state is accomplished within 20 revolutions corresponding to a time 0.4 sec from the begin.

K.V. Avramov, O. Borysiuk, [6], suggested a general approach for analysis the vibration of one disk rotor in arbitrary length journal bearings.

They used the finite element method in the solution of Reynolds equation.

The self-sustained vibration of the rotor was analyzed by using the harmonic balance and the continuation methods.

They investigated the effect of the fluid viscosity and bearing clearance on the self-sustained vibration and the rotor stability. They found that the amplitudes of the self-sustained vibration increase with the increase of the clearance in bearing.

Thomas Wirsing, [7], Studied the effect of axially oscillating journal bearing on the stiffness and damping coefficients. He achieved the axial oscillation of the bearing by using a magnetic actuator and this motion caused the varying in the stiffness and damping from non-oscillating bearing.

This study is useful to reduce the failure caused by the phenomenon of decreased lubricant viscosity due to temperature increase.

M. Lahmar, et al. [8] analyzed the non-dynamic of laminar and turbulent journal bearing with and without unbalanced forces.

Using an approximate method named the optimized short bearing theory. The method based on the separation of variable of pressure distribution in axial direction. The results were compared with those obtained by Ockvirck approximation.

They found that the maximum oil film pressure is half the value obtained by Ockvirck solution. Also they showed that the optimized method is good for reducing the required time for dynamic analysis without loss the accuracy.

They concluded that this method is a useful tool to analyze the hydrodynamic journal bearing especially for the aspect ratios less than 1.

Omidreza Ebrat, et. al, [9], presented a new formulation based on a local perturbation of the oil film at each node of the discretized domain.

The analysis included the effect of journal misalignment and deformation of bearing structural in rotor dynamics.

They used the finite difference method in solving the Reynolds equation using a successive Over Relaxation (SOR) technique. The result of this

research were the oil film pressure and dynamic characteristic including stiffness and damping effect.

They noticed that, this analysis is useful for engine dynamic crankshaft-block interaction studies with flexible crankshaft and block structures.

N. K. Rana, et. al, [10], Presented an approximate method for short bearing to show the effect of micro polar turbulent flow condition on the dynamic behavior.

They modified the Reynolds equation to incorporate turbulence and micro polar fluid parameter to determine the static and dynamic characteristics for turbulent flow.

The modified Reynolds equation is achieved by taking into account the influence of the non-Newtonian behavior. They used the finite difference method to discretize the Reynolds equation and solved by Gauss- seidel iteration with the over relaxation factor.

They found that, for turbulent flow, the bearing is highly stable at high Reynolds number and at high speed.

The analysis of this research can be used to analyze the stability of the journal bearing.

To our knowledge there is no research was done about the effect of harmonic forced vibration on the performance of the hydrodynamic journal bearing.

MATHEMATICAL MODELING

In this chapter the Reynold equation with a suitable boundary and initial condition has been developed to solve the problem. The mathematical and numerical modeling using finite difference method is presented. The computer program (FORTRAN 95) has been utilized to obtain the results.

3.1 Geometry of journal bearing

The geometry of journal bearing is describe as shown in the figure (3.1).

o_b – bearing center

o_j – journal center

e – eccentricity

Produce line ($o_j o_b$) to meet bearing surface at G, this is the position of maximum film thickness and from this part the angle θ is measured. At line oc meets the bearing surface at F which is the position of minimum film thickness.

$o_b a - R_1$ - radius of bearing

$o_j a = R_1 + h$

$c = R_1 - R$

where c is a radial clearance

h_{\min} - minimum film thickness at F = $c - e$

h_{\max} - maximum film thickness at G = $c + e$

ε - eccentricity ratio = e/c

When shaft and bearing are concentric $e = 0 \longrightarrow \varepsilon = 0$

When the shaft and bearing are touch $e = c \longrightarrow \varepsilon = 1$

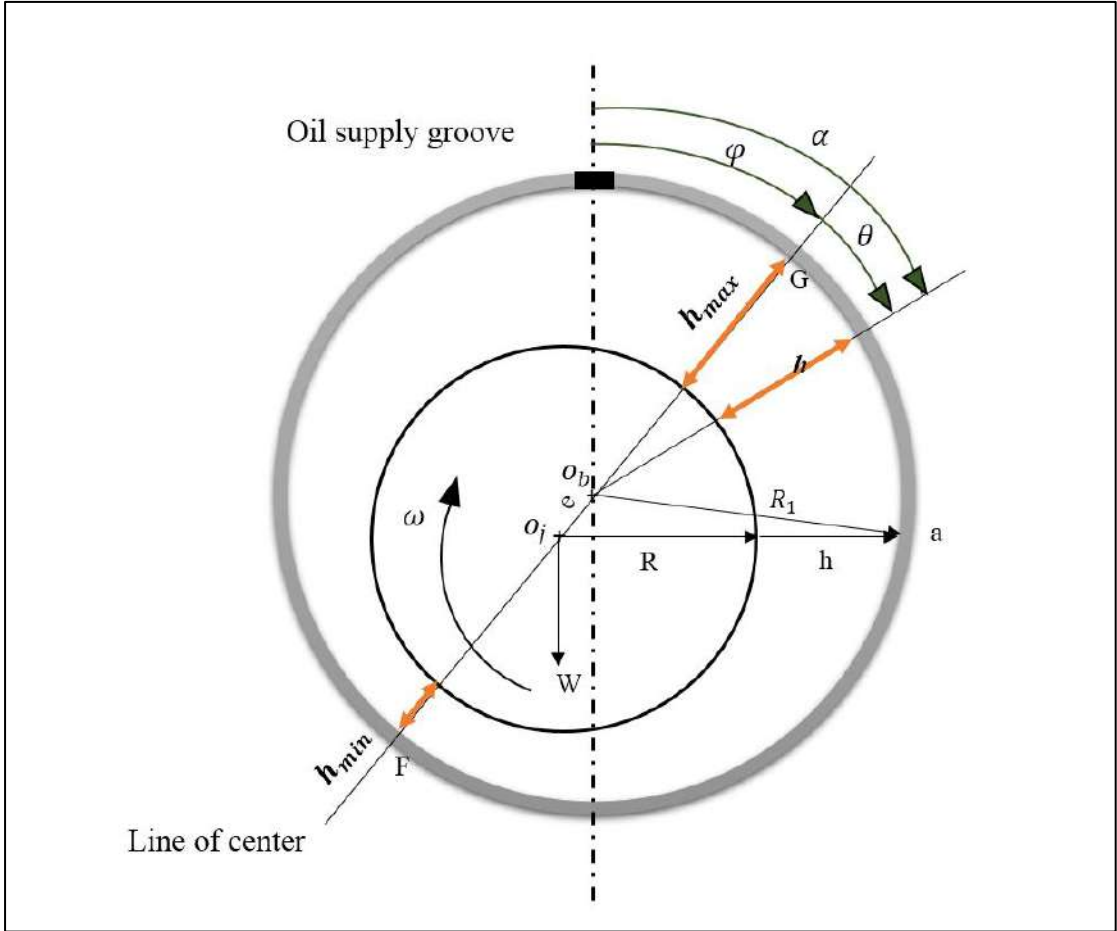


Figure (3-1) Geometry of Journal Bearing

3.2 Coordinate of the system

The global coordinates system used is assumed to be cartesian (x , y , z) with the original point fixed to bearing bush center, as shown in figure (3.2)

The x - coordinate is in the circumferential direction, y - coordinate across the oil film thickness, and the (z) coordinate in the axial direction, across the length of bearing perpendicular to the plane of (x , y)

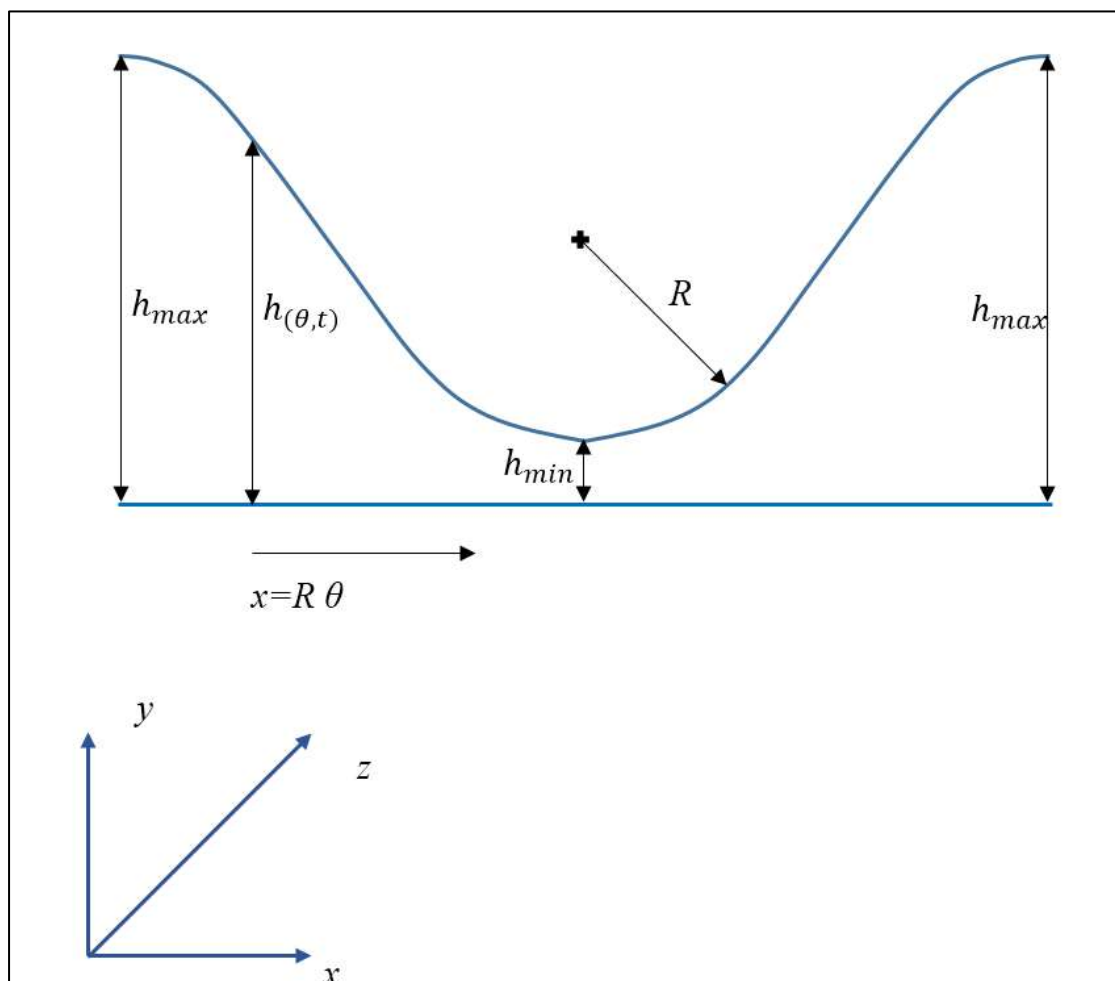


Figure (3-2) Oil film thickness and coordinate of the system of journal bearing

3.3 Reynolds equation

The Reynolds equation for the laminar flow of an isoviscous incompressible fluid is derived as reported by [1]:

$$\frac{\partial}{\partial x} \left(h^3 \frac{\partial p}{\partial x} \right) + \frac{\partial}{\partial z} \left(h^3 \frac{\partial p}{\partial z} \right) = 6\mu u \frac{\partial h}{\partial x} + 12\mu \frac{\partial h}{\partial t} \quad (3.1)$$

In this work, it is considered the short bearing approximation for the solution of the Reynolds equation. The short bearing theory is useful for length of bearing to diameter of shaft ratio up to $(L/D \leq 1)$, Dubois and Ocivirk, 1953. With $\partial p / \partial x = 0$, hence, the first term on the left hand side of equation (3.1) is removed. The Reynolds equation for an infinitely short journal bearing is written as,

$$\frac{\partial}{\partial z} \left(h^3 \frac{\partial p}{\partial z} \right) = 6\mu u \frac{\partial h}{\partial x} + 12\mu \frac{\partial h}{\partial t} \quad (3.2)$$

3.4 Steady state analysis

For steady-state of Reynolds equation, the second term of the right hand of equation (3.2) is neglected and takes the form:

$$\frac{\partial}{\partial z} \left(h^3 \frac{\partial p}{\partial z} \right) = 6\mu u \frac{\partial h}{\partial x} \quad (3.3)$$

The oil film thickness can be evaluated as described by [11] as:

$$h(\theta) = c(1 + \varepsilon \cos\theta) \quad (3.4)$$

By integration equation. (3.3) twice gives the pressure distribution function

$$p = \frac{3\mu u}{h^3} \frac{\partial h}{\partial x} z^2 + Az + B \quad (3.5)$$

Where A and B are the integration constants to be determined by applying the boundary conditions, where the z axis is chosen to be in the

center of the bearing so that the boundary conditions which were used can be expressed as described by [11] is

At the journal bearing edges

$$p = p_{atm} = 0 \quad \text{at } \theta = 0.2\pi \text{ and } z = \pm \frac{l}{2} \quad (3.6)$$

Applying these boundary conditions results in

$$A = 0$$

$$B = -\frac{3\mu u \partial h l^2}{h^3 \partial x 4}$$

Differentiating equation (3.4) with respect to x and substitute $x = R\theta$,

$$\frac{\partial h}{\partial x} = \frac{-c\varepsilon \sin \theta}{R} \quad (3.7)$$

substitute equation (3.7) into equation (3.5) yield,

$$p = \frac{3\mu u \varepsilon \sin \theta}{Rc^2(1 + \varepsilon \cos \theta)^3} \left(\frac{l^2}{4} - z^2 \right) \quad (3.8)$$

Where

$$u = \omega R$$

Equation (3.8) gives the dimensional form of pressure distribution in the axial direction.

3.5 Dynamic analysis

The dynamic effect in tribology mean to take in to account the term $(\partial h/\partial t)$ in Reynolds equation. In this thesis the dynamic effect is considered to be generated from two sources, namely

1. Self-excitation
2. Forced harmonic excitation

3.5.1 Self excitation

For dynamically loaded short journal bearing the position of the journal is defined by the eccentricity e and the angle θ . For an eccentric journal bearing, the angle θ can be expressed as

$$(\theta = \alpha - \varphi) \quad (3.9)$$

hence the oil film thickness equation will be

$$h(\theta, t) = c(1 + \varepsilon(t)\cos\theta) \quad (3.10)$$

Differentiating equation (3.10) with respect to x and t

$$\begin{aligned} \frac{dh}{dx} &= -c\varepsilon\sin\theta \frac{d\theta}{dx} \\ \frac{dh}{dx} &= \frac{-c\varepsilon\sin\theta}{R} \end{aligned} \quad (3.11)$$

And

$$\frac{\partial h}{\partial t} = -c\varepsilon\sin\theta \frac{d\theta}{dt} + c\dot{\varepsilon}\cos\theta$$

From equation (3.9)

$$\begin{aligned} \frac{d\theta}{dt} &= -\frac{d\varphi}{dt} = -\dot{\varphi} \\ \frac{\partial h}{\partial t} &= c(\varepsilon\sin\theta\dot{\varphi} + \dot{\varepsilon}\cos\theta) \end{aligned} \quad (3.12)$$

Substitute equation (3.11) and (3.12) in to equation (3.2) yield:

$$\frac{\partial}{\partial z} \left(h^3 \frac{\partial p}{\partial z} \right) = -6\mu\omega c \varepsilon \sin\theta + 12\mu c (\varepsilon \dot{\phi} \sin\theta + \dot{\varepsilon} \cos\theta) \quad (3.13)$$

Integrating equation (3.13) twice and applying the boundary condition of (3.6), the equation of pressure distribution under self-excitation will be.

$$p = \frac{6\mu c}{h^3} [\dot{\varepsilon} \cos\theta + \varepsilon(\dot{\phi} - \bar{\omega}) \sin\theta] \left(z^2 - \frac{l^2}{4} \right) \quad (3.14)$$

Where ($\bar{\omega} = \omega/2$).

3.5.2 Forced harmonic excitation

When the journal bearing is subjected to external vibration such as a harmonic excitation then the response will take the form of the particular integral.

The particular integral represents the response of the system to forced vibration, as expressed by [12], as,

$$h_2(t) = H_2 \sin(\omega t - \psi) \quad (3.15)$$

Where

H_2 and ψ are the amplitude of oscillation and the phase angle of the displacement with respect to the exciting force, respectively

$$H_2 = \frac{F_o}{K \sqrt{\left[1 - \left(\frac{\omega}{\omega_n} \right)^2 \right]^2 + \left[2\xi \frac{\omega}{\omega_n} \right]^2}} \quad (3.16)$$

$$\psi = \tan^{-1} \frac{2\xi \frac{\omega}{\omega_n}}{1 - \left(\frac{\omega}{\omega_n} \right)^2} \quad (3.17)$$

where

$\frac{\omega}{\omega_n}$ – frequency ratio

To find the value of the stiffness (K) by considering the journal bearing as a simply support beam and used the double integration method as shown in appendix [A] obtained that,

$$\omega_n = \sqrt{\frac{48EI}{ML^3}} \quad (3.18)$$

$$K = \frac{48EI}{L^3} \quad (3.19)$$

Assuming that, under external vibration the oil film thickness will be

$$h_v = h_1 + h_2 \quad (3.20)$$

Where

$$h_1 = c(1 + \varepsilon \cos\theta)$$

$$h_2 = H_2 \sin(\omega t - \psi)$$

The new equation of the oil film thickness in case of harmonic excitation will be,

$$h_v(\theta, t) = c(1 + \varepsilon \cos\theta) + H_2 \sin(\omega t - \psi) \quad (3.21)$$

A gain for the right hand side of equation (3.2),

$$\frac{dh_v}{dx} = \frac{dh}{dx} \quad (3.22)$$

$$\frac{\partial h_v}{\partial t} = c(\varepsilon \sin\theta \dot{\varphi} + \dot{\varepsilon} \cos\theta) + \omega H_2 \cos(\omega t - \psi) \quad (3.23)$$

Then by using the boundary condition of (3.6) and substitute equations (3.22) and (3.23) in to equation (3.2), gives the oil film pressure distribution of journal bearing subjected to external vibration,

$$p = \frac{6\mu}{h^3} [c\dot{\varepsilon} \cos\theta + c\varepsilon \sin\theta (\dot{\varphi} - \bar{\omega}) + \omega H_2 \cos(\omega t - \psi)] \left(z^2 - \frac{L^2}{4} \right) \quad (3.24)$$

3.6 Load Carrying Capacity

Consider a small segment, $Rd\theta dz$, at any angle θ to the line of centers, the fluid reaction force that equilibrates the applied load is $pRd\theta dz$. The force components in the direction of line of centers of the journal $W_{\bar{x}}$ and the normal to the line $W_{\bar{y}}$ which can be evaluated by integrating the pressure around the journal bearing.

3.6.1 Load Carrying Capacity of Steady state

The load components resulting from the pressure development tangent and normal to the line of centers under the half Sommerfeld assumption for steady condition can be written as

$$W_{\bar{x}} = 2R \int_0^{\pi L/2} \int_0^{\pi L/2} p \cos \theta d\theta dz \quad (3.25)$$

$$W_{\bar{y}} = 2R \int_0^{\pi L/2} \int_0^{\pi L/2} p \sin \theta d\theta dz \quad (3.26)$$

Substitute equation (3.8) in to equations (3.25) and (3.26) with using the individual integrals expressed by [11] the force components can obtain as

$$W_{\bar{x}} = -\frac{u\mu\varepsilon^2 L^3}{c^2(1-\varepsilon^2)^2} \quad (3.27)$$

$$W_{\bar{y}} = \frac{\pi u\mu\varepsilon L^3}{4c^2(1-\varepsilon^2)^{3/2}} \quad (3.28)$$

Then the resultant load,

$$W = \sqrt{W_{\bar{x}}^2 + W_{\bar{y}}^2} \quad (3.29)$$

The resultant load can be expressed in the non-dimension form as

$$\bar{W} = \frac{\pi\varepsilon}{(1-\varepsilon^2)^2} \left[\varepsilon^2 \left(\frac{16}{\pi^2} - 1 \right) + 1 \right]^{1/2} \quad (3.30)$$

Where

$$\bar{W} = \frac{4Wc^2}{\mu u L^3}$$

3.6.2 Load Carrying Capacity of Dynamic Condition

For dynamically loaded journal bearing the full sommerfeld is used [13]. The tangential and normal components of the load carrying capacity will be:

$$W_{\bar{x}} = W \cos \varphi = 2R \int_0^{2\pi} \int_0^{L/2} p \cos \theta d\theta dz \quad (3.31)$$

$$W_{\bar{y}} = W \sin \varphi = 2R \int_0^{2\pi} \int_0^{L/2} p \sin \theta d\theta dz \quad (3.32)$$

respectively, and

$$\varphi = \tan^{-1}\left(-\frac{W_{\bar{y}}}{W_{\bar{x}}}\right) \quad (3.33)$$

Substitute equation (3.14) in to equations (3.31) and (3.32) and using the individual integral described by [13], it leads to

$$W \cos \varphi = -\frac{\pi\mu RL^3}{c^2} \left[\frac{(1 + 2\varepsilon^2)}{(1 - \varepsilon^2)^{5/2}} \right] \frac{\partial \varepsilon}{\partial t} \quad (3.34)$$

$$W \sin \varphi = \frac{\pi\mu RL^3}{c^2} \left[\frac{\varepsilon}{(1 - \varepsilon^2)^{3/2}} \right] (\bar{\omega} - \dot{\varphi}) \quad (3.35)$$

From equations (3.34) and (3.35) the locus of the journal center velocity and the velocity of journal center can be expressed as

$$\dot{\varepsilon} = -\frac{(W \cos \varphi)c^2}{\pi\mu RL^3} \left[\frac{(1 - \varepsilon^2)^{5/2}}{(1 + 2\varepsilon^2)} \right] \quad (3.36)$$

$$\dot{\varphi} = \bar{\omega} - \frac{(W \sin \varphi)c^2}{\pi\mu RL^3} \left[\frac{(1 - \varepsilon^2)^{3/2}}{\varepsilon} \right] \quad (3.37)$$

respectively.

As the journal bearing is exposed to self-excited vibration due to cyclic load [4], have

$$W = W_o \sin(\omega t) \quad (3.38)$$

Substitute equation (3.38) in equations (3.36) and (3.37) obtained

$$\dot{\varepsilon} = -\frac{(W_o \sin(\omega t)) \cos \varphi c^2 \left[\frac{(1 - \varepsilon^2)^{5/2}}{(1 + 2\varepsilon^2)} \right]}{\pi \mu R L^3} \quad (3.39)$$

$$\dot{\varphi} = \bar{\omega} - \frac{(W_o \sin(\omega t)) \sin \varphi c^2 \left[\frac{(1 - \varepsilon^2)^{3/2}}{\varepsilon} \right]}{\pi \mu R L^3} \quad (3.40)$$

Equation (3.39) describes the locus of the journal center under the imposed cyclic load. The eccentricity ratio, ε , depends upon the initial position of the journal center.

Equation (3.40) represented the velocity of the journal center.

3.7 Numerical analysis

The non-dimensional form of Reynold's equation (3.2) with constant viscosity is described as:

$$\bar{h}^3 \left(\frac{R}{L} \right)^2 \frac{\partial}{\partial \bar{z}} \left(\frac{\partial \bar{P}}{\partial \bar{z}} \right) = \frac{\partial \bar{h}}{\partial \theta} + 2 \frac{\partial \bar{h}}{\partial T} \quad (3.41)$$

Where:

$$\bar{P} = \frac{p}{6\mu\omega} \left(\frac{c}{R} \right)^2 \quad \bar{z} = \frac{z}{l} \quad \theta = \frac{x}{R} \quad T = \frac{tu}{R} \quad (3.42)$$

$$\bar{h} = \frac{h}{c} = (1 + \varepsilon \cos\theta) \quad (3.43)$$

The dimensionless governing differential equation described above is solved by using the finite difference quotients to get the pressure distribution in the oil film.

3.7.1 Mesh generation

The dimensionless oil film pressure distribution can be also obtained by solving equation (3.39), which can be greatly simplified by a well – constructed grid. For short bearing approximation and for 2-D finite difference analysis, a grid size is chosen to be of (n) in circumferential direction, θ and (m) in axial direction, z, as shown in the figure (3.3) The central technique in the finite difference method is adopted.

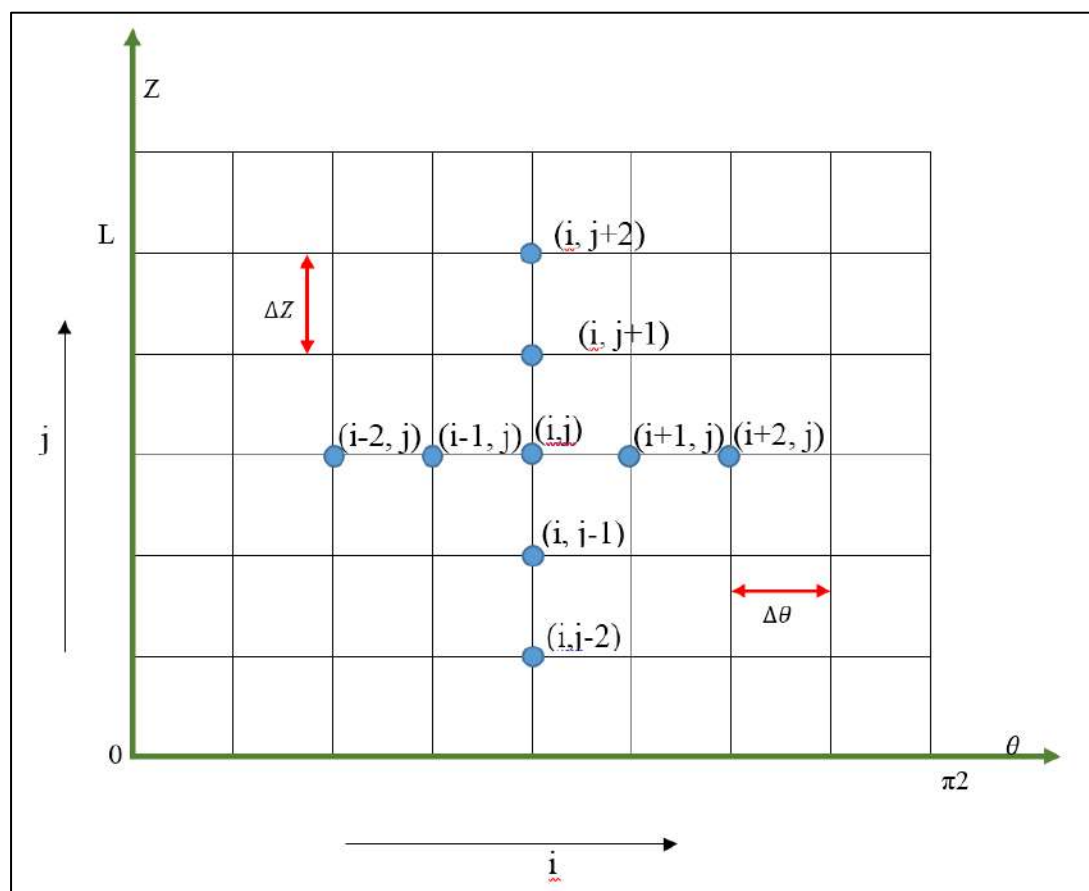


Figure (3.3) Discretization of oil film domain

$$1 \leq i \leq n$$

$$1 \leq j \leq m$$

Define the mesh size in circumferential direction (Δx) and along the bearing length (Δz), as

$$\Delta x = \frac{2\pi R}{n-1} \quad (3.44)$$

$$\Delta z = \frac{L}{m-1} \quad (3.45)$$

Which can be expressed in dimensionless group as

$$\Delta \theta = \frac{\Delta x}{R} \quad (3.46)$$

$$\Delta \bar{z} = \frac{\Delta z}{L} \quad (3.47)$$

3.7.2 Solving the Reynold's Equation

To get the pressure distribution (\bar{P}) through the oil film, the grid points are taken in the coordinates of θ and \bar{z} to make it suitable for the finite difference method.

For any point in the oil film mesh (i, j), the Reynold equation can be written:

$$\begin{aligned} \bar{h}^3_{i,j} \left(\frac{R}{L}\right)^2 \left(\frac{\bar{P}_{i,j+1} - 2\bar{P}_{i,j} + \bar{P}_{i,j-1}}{\Delta \bar{z}^2}\right) \\ = \frac{\bar{h}_{i+1,j} - \bar{h}_{i-1,j}}{2\Delta \bar{x}} + 2 \left(\frac{\bar{h}_{i,j}^{n+1} - \bar{h}_{i,j}^n}{\Delta T}\right) \end{aligned} \quad (3.48)$$

$$\begin{aligned} (\bar{P}_{i,j+1} - 2\bar{P}_{i,j} + \bar{P}_{i,j-1}) = \left[\left(\frac{\bar{h}_{i+1,j} - \bar{h}_{i-1,j}}{2\Delta \bar{x}}\right) + 2 \left(\frac{\bar{h}_{i,j}^{n+1} - \bar{h}_{i,j}^n}{\Delta T}\right) \right] \\ \left[\frac{(L/R)^2 \Delta \bar{z}^2}{\bar{h}^3_{i,j}} \right] \end{aligned} \quad (3.49)$$

Rearranging equation (3.49) for $\bar{P}_{i,j}$:

$$\begin{aligned} \bar{P}_{i,j} = \left[\frac{\bar{P}_{i,j+1} + \bar{P}_{i,j-1}}{2} \right] - \left[\left(\frac{\bar{h}_{i+1,j} - \bar{h}_{i-1,j}}{2\Delta \bar{x}}\right) + 2 \left(\frac{\bar{h}_{i,j}^{n+1} - \bar{h}_{i,j}^n}{\Delta T}\right) \right] \\ \left[\frac{(L/R)^2 \Delta \bar{z}^2}{\bar{h}^3_{i,j}} \right] \end{aligned} \quad (3.50)$$

The equation above gives the dimensionless oil film pressure in the circumference and axial directions.

For steady state condition the part which related to time assumed to be zero, so equation (3.50) can rewrite:

$$\bar{P}_{i,j} = \left(\frac{\bar{P}_{i,j+1} + \bar{P}_{i,j-1}}{2} \right) - \left(\frac{\bar{h}_{i+1,j} - \bar{h}_{i-1,j}}{2\Delta\bar{x}} \right) \left(\frac{(L/R)^2 \Delta\bar{z}^2}{2\bar{h}_{i,j}^3} \right) \quad (3.51)$$

3.7.3 Solution procedure of steady state case

The following steps are used to obtain the pressure distribution in the oil film at the mid – plane of the bearing ($z=0$).

- 1) The pressure of oil film at the grid points of bearing bush and shaft is assumed.
- 2) The dimensionless value of oil film thickness (\bar{h}) is calculated from equation (3.43)
- 3) Applying the boundary condition equation (3.6) where the value of pressure assumed to be zero at the boundary of bearing bush.
- 4) Calculate the dimensionless pressure of oil film of all nodes of grid using equation (3.51), the negative pressure is assumed to be zero during the computation according to half Sommerfeld boundary condition.
- 5) When the converging criteria for pressure equation reached to (10^{-6}), the iterations are stopped. The converging criteria can be calculating as describe by [16]

$$\frac{\sum |\bar{P}_{i,j} - \bar{P}_{i,j}^{old}|}{\sum |\bar{P}_{i,j}|} < 10^{-6} \quad (3.52)$$

- 6) Calculating the load carrying capacity using equations (3.30).

3.7.4 Solution procedure of combined effect of the self excited and forced harmonic vibration.

The following steps are used to obtain the pressure distribution in the oil film at the mid – plane of the bearing ($z=0$).

- 1) Assuming the time steps and the total time required.
- 2) Assuming the initial value of the eccentricity ratio and the attitude angle from the steady state case as a first step of the solution procedure.
- 3) Applying the initial condition, i.e, at time equal to zero the oil film pressure is equal to the value of oil film pressure obtained from the steady condition.
- 4) Assuming a value for applied load, then calculating a new values of eccentricity ratio using equation (3.39).
- 5) Calculating the dimensionless value of oil film thickness (\bar{h}) from equation (3.43) for the calculated value of eccentricity ratio.
- 6) Applying the boundary condition equation (3.6).
- 7) Calculating the dimensionless pressure of oil film for each node from equation (3.50), the negative pressure is assumed to be zero during the computation.
- 8) Calculate the load carrying capacity numerically by integrated the oil film pressure over the area of nodes as follows

$$W_{i,j} = P_{i,j}A_{i,j} \quad (3.53)$$

$$W_{i,j} = A_{i,j} \sum P_{i,j} \quad (3.54)$$

Where

$$A_{i,j} = \Delta x_i \Delta z_j$$

Which is the same for all element.

until the calculated load equal to the assumed load.

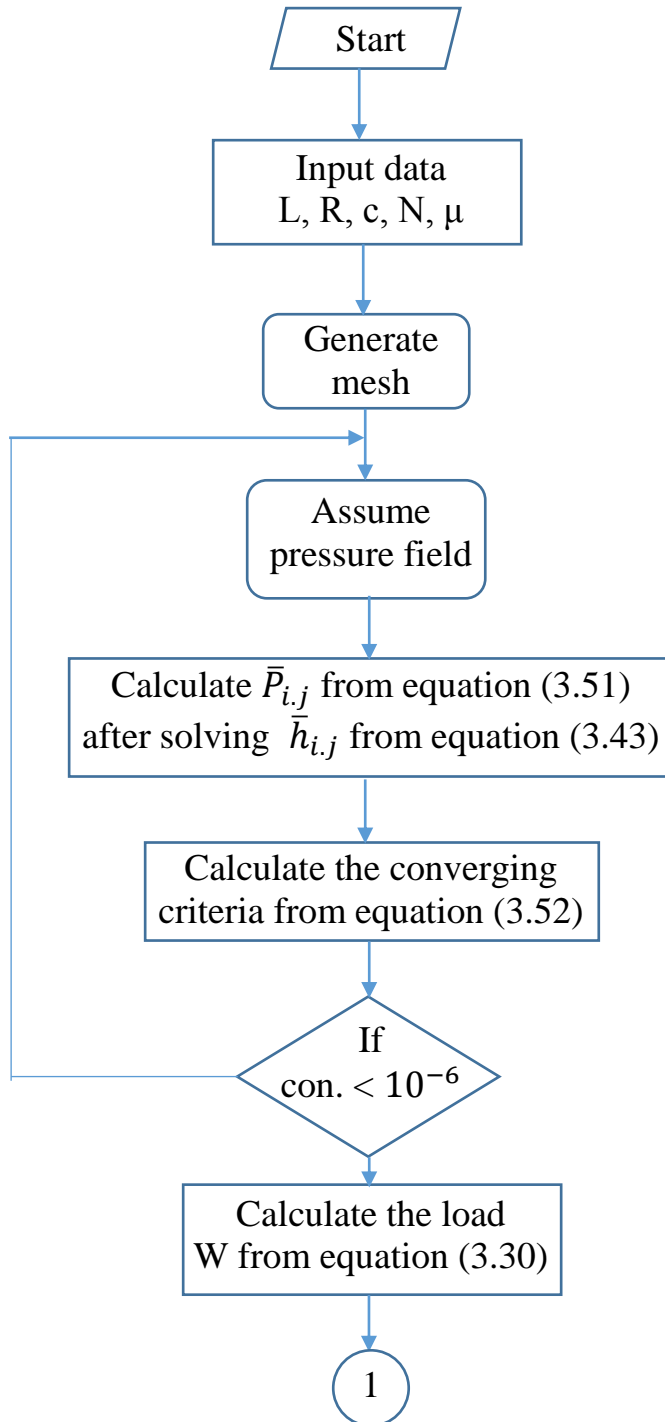
- 9) The iteration are stopped when the converging criteria for pressure equation reached to (10^{-6}) , using equation (3.52).
- 10) When the system subjected to external harmonic exaction, the stiffness, the natural frequency of the system, the amplitude and the phase angle of vibration, using equations (3.19), (3.18), (3.17), (3.16) are calculated respectively.
- 11) The oil film thickness is re calculated using equation (3.21).
- 12) The same steps (6 – 9) are repeated to obtain the pressure distribution under the effect of combination of self and external expiation.
- 13) In the case of calculating the pressure distribution of oil film due to harmonic excitation only, the steps from (6-12) are proceeded only.

3.8 Computer program

To solve the Reynold equations numerically, a suitable computer program is written using (FORTRAN – 95) computer language.

The computer program flow chart for the steady state and the dynamic cases are shown in the figures (3.4) and (3.5) respectively.

1) Flowchart of Computer program for steady state condition



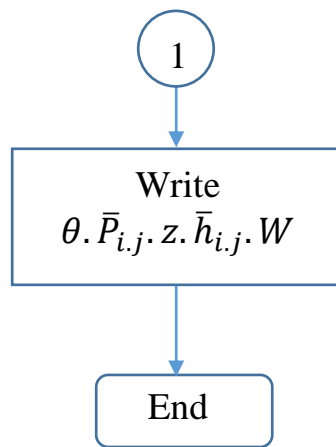
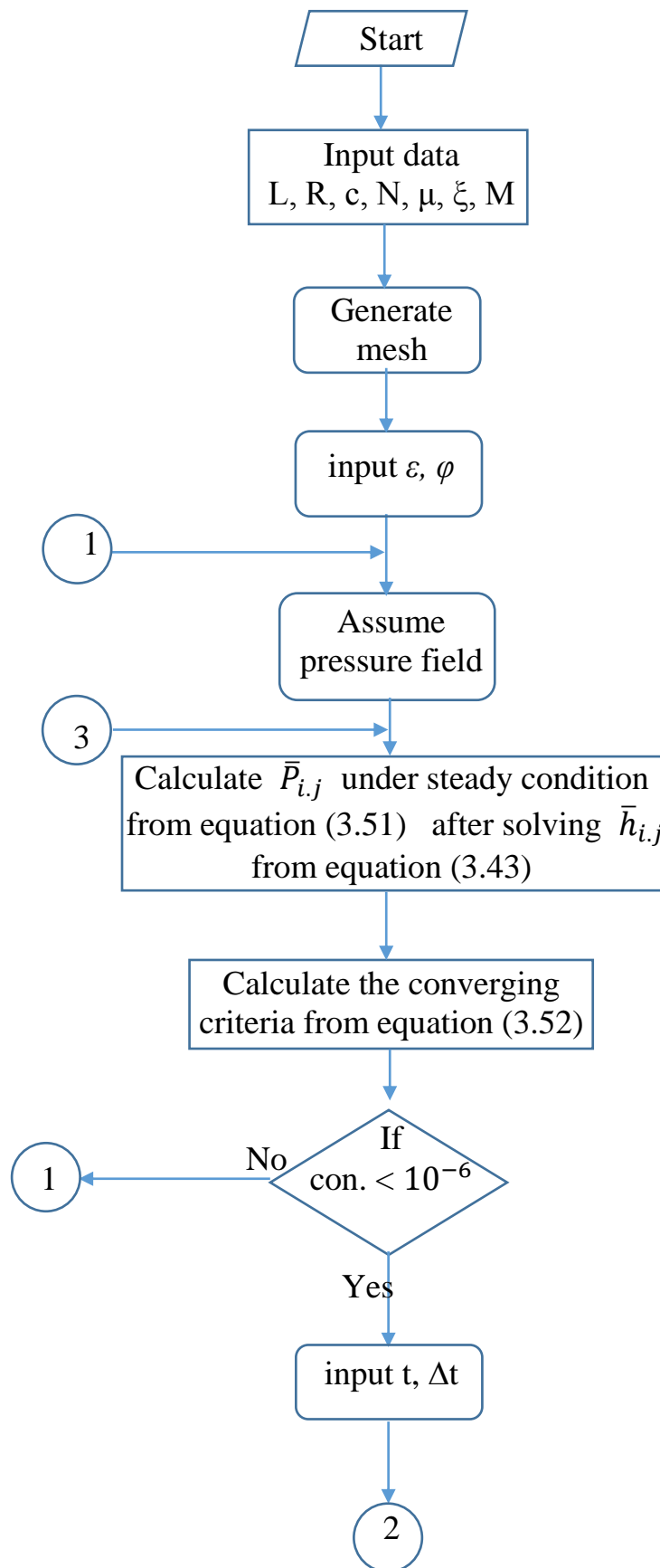
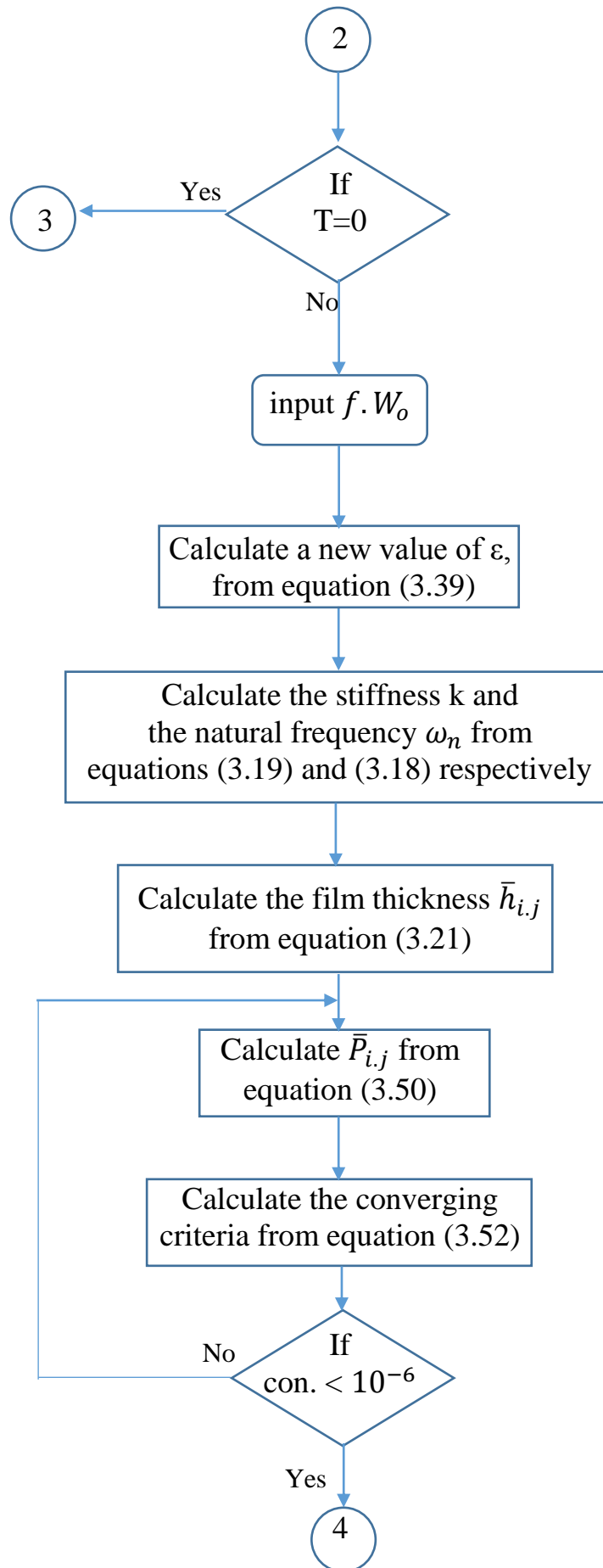


Figure (3.4) Flowchart of program for steady state

2) Flowchart of Computer program of vibration condition





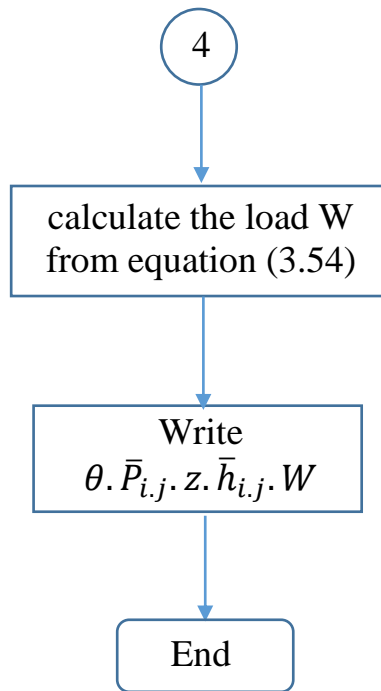


Figure (3.5) Flowchart of program for dynamic condition

EXPERIMENT STUDY

4.1 Technical Description

The experimental work explains the implementation and assembly of the Journal Bearing apparatus to for investigating the distribution of pressure. This apparatus is available in the mechanical engineering laboratories in the university of Kerbala. The distribution of pressure and the load carrying capacity can be determined on a sliding bearing model at different bearing loads and speeds. The sliding contact bearing consists of a journal bearing driven by an electrical motor. The radial distribution of pressure can be recorded in the bearing gap at 10 measuring points around its bearing and 10 to record the temperature.

4.2 Journal Bearing Set-up

The test rig journal bearing consists of many parts, bush, shaft, hosing, brackets, coupling, foundation, thermocouples sensor, manometer tubs, loading system, motion system, lubricant system and main table as shown in the figure (4-1).

The bush, shaft and housing was manufactured by the (General Company for Mechanical Industries in Iskandaria, Babil, Iraq).

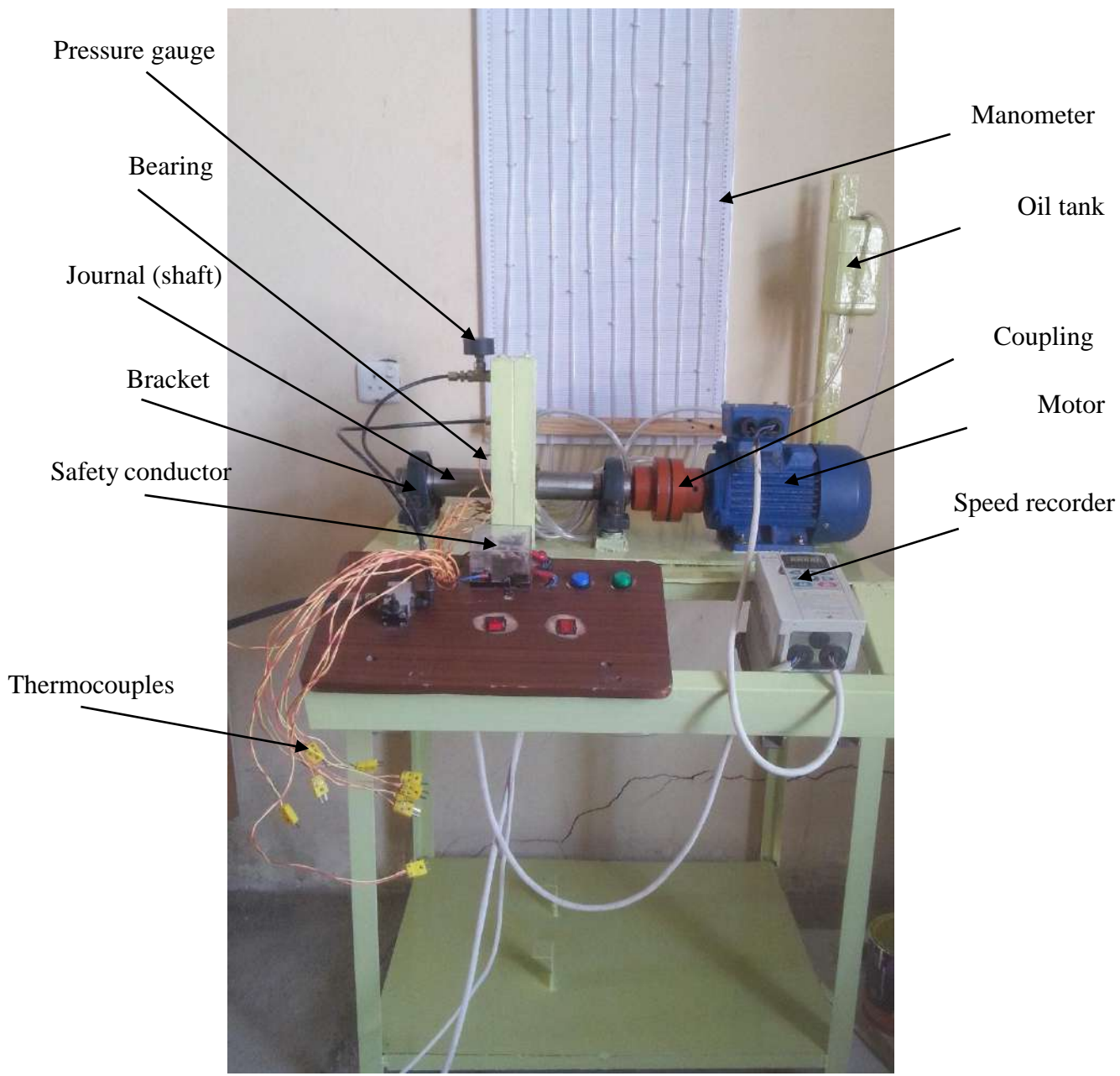


Figure (4-1) Journal bearing apparatus

4.2.1 Bush

The specifications of the bush are

- 1- the metal is brass
- 2- inside diameter 50.2 mm
- 3- outside diameter 67mm
- 4- length of bush 49.8 mm
- 5- it contains 20 holes with diameter 2mm. Ten for measuring the pressure the other ten for measuring the temperature as shown in the figure (4-2b).
- 6- it contains two holes of 5mm diameter for supply and drainage lubricant as shown in the figure (4-2d).
- 7- it contains a groove to circulate the lubricant oil.

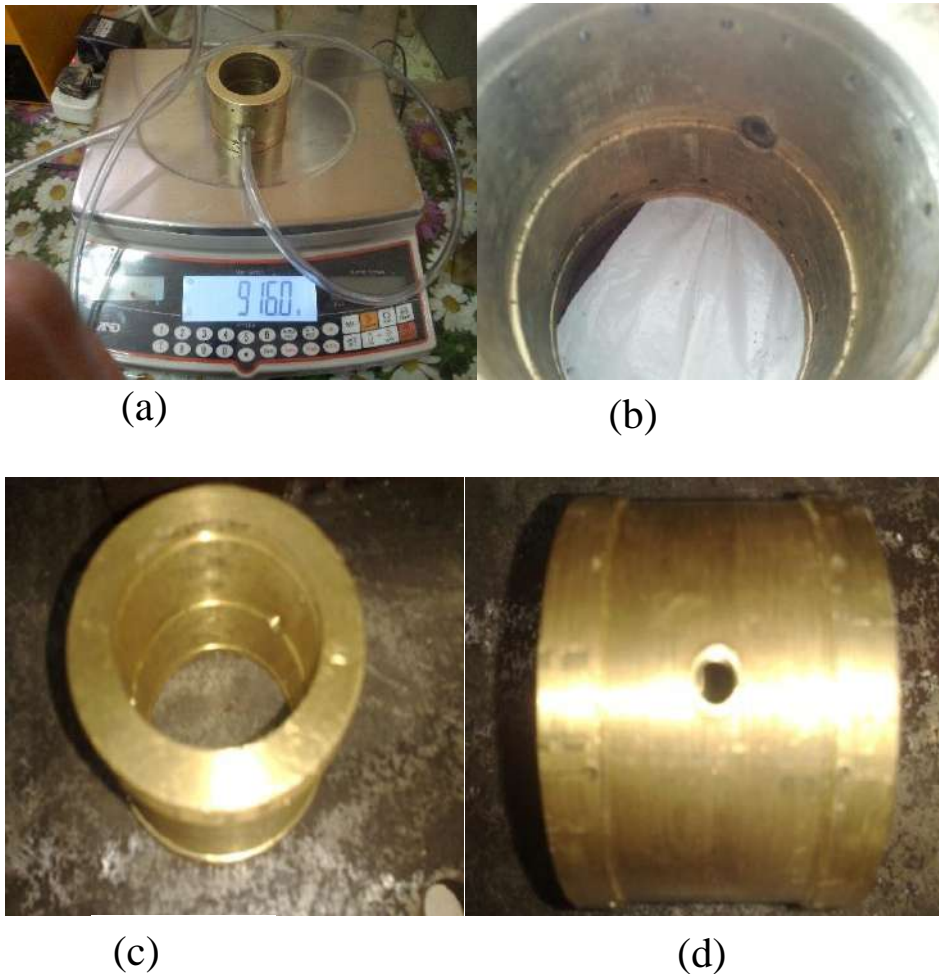


Figure (4-2) The bearing bush

4.2.2 The shaft

The specifications of the shaft are

1. the metal is st45
2. diameter 50 mm
3. length 400mm
4. one end has diameter of 40mm with length 60mm and other end of 35mm diameter with length 70mm
5. the shaft has hardness (45-50) hvrs
6. the shaft has a key way with length of 70mm and width of 10mm, for connecting to the coupling.

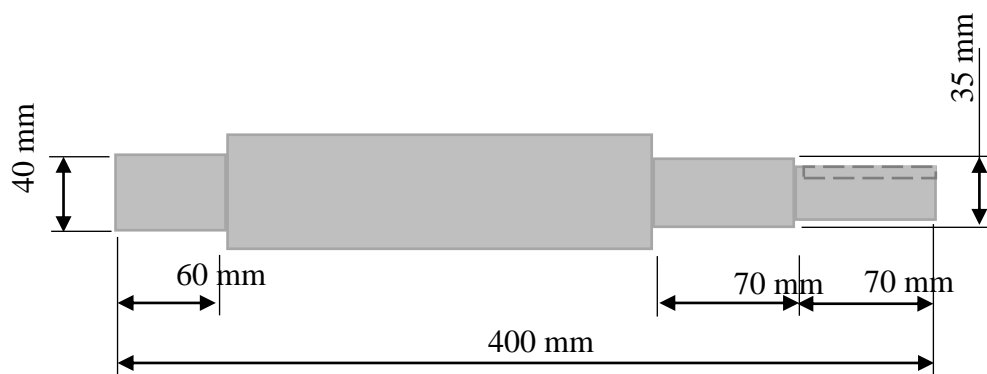


Figure (4-3) Schematic of the shaft



Figure (4-4) The journal (shaft).

4.2.2 The hosing

The hosing has the following specifications

- 1- the metal is brass
- 2- hosing has two equal halves
- 3- inside diameter 68mm
- 4- each half of hosing has rectangular cross section area (200×100) mm and thickness 35mm as shown in the figure (4-6).
- 5- hosing has two holes with 10mm diameter for oil lubricant tubes
- 6- hosing has two holes with 17mm diameter for joining the two halves of hosing

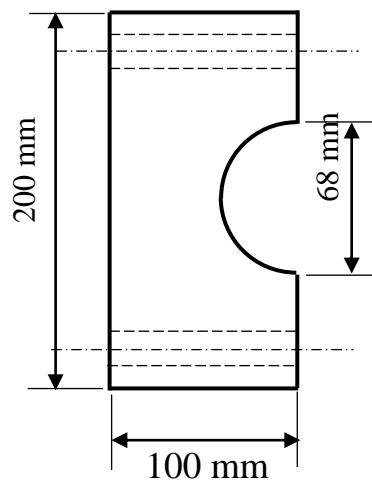


Figure (4-5) Schematic of housing



Figure (4-6) The housing

4.2.2 Brackets

Two brackets lubricated by grease with diameter 40mm and length 60mm from UCB company. There are used to support the shaft as shown in the figure (4-7).



Figure (4-7) The brackets

4.2.2 Coupling

The coupling is used for connecting the shaft with the motor as shown in the figure (4-8).



Figure (4-8) The coupling

4.3 Measurement element

The test rig has two measuring element. One of them is the manometer to measure the pressure. The second is the thermocouples to measure the temperature of the lubricant.

4.3.1 Manometer tubs

The measurements of lubricant pressure are displayed by means of 10 plastic tube manometers mounted on a board of dimension (2000×500) mm. The manometers tube has (6) mm diameter of length (2000) mm as shown in the figure (4-9)



Figure (4-9) The manometer device

The pressure was measured by the height of the lubricant in the manometer tubes using a liquid formula

$$P = \rho g h_c \quad (4-1)$$

Where

ρ - density of the lubricant

g - acceleration due to gravity

h_c - height of the column of the lubricant

4.3.2 Thermocouples

Ten Thermocouples type (K) are distributed around the bush circumference are used to observe the lubricant temperature.

Temperature recorder (model, BTM- 4208SD, 12 channels, SD storage, accuracy $0.1 \% \pm 0.1 \text{ }^{\circ}\text{C}$) was used to read thermocouples where it's stored in SD storage. The saving data will present into the EXCEL software.



Figure (4-10) Thermocouples type K

4.4 Loading system

The loading system has a maximum load of 88 kg. It's contain the following part

- 1- pneumatic jig with 24mm stroke & 39mm bore as shown in the figure (4-11)
- 2- electrical compressor with power (1/6 hp) and 500 psi air pressure as shown in the figure (4-12)
- 3- solenoid valve as shown in the figure (4-14)
- 4- 15 bar pressure gauge as shown in the figure (4-13)
- 5- connectors & pressure pipes



Figure (4-11) Pneumatic jig



Figure (4-12) Electrical compressor



Figure (4-13) Pressure gauge



Figure (4-14) Solenoid valve

4.5 driving system

The driving system has the following component:

- 1- 3-phase motor 2hp 3000 rpm as shown in the figure (4-15).
- 2- input single-phase output 3-phase,
- 3- speed recorder with frequency range from zero to 60 Hz, as shown in the figure (4-16)
- 4- safety conductor 120 A, as shown in the figure (4-17)



Figure (4-15) 3-phase motor



Figure (4-16) Speed recorder



Figure (4-17) Safety conductor

4.6 Lubricant system

The lubricant system has a (1) liter oil reservoir, connections pipes and (1) m stand as shown in the figure (4-18).

The specification of the oil used was reported by Al- Dora Refinery – Iraq. Appendix (C).



Figure (4-18) oil reservoir

The whole system of journal bearing is rested on four legs table of height (1200) mm (800) mm length and (650) mm width.

RESULTS AND DISCUSSIONS

The experimental and numerical results of steady state and dynamic conditions under the effect of forced vibration of short length journal bearing are discussed in this chapter.

The operating parameters namely, rotational speed, applied load, type of lubricate and eccentricity ratio effects on the short bearing are discussed.

The bearing characteristic are presented in tables (5-1) and (5-2).

Table (5-1) The journal bearing characteristic of experimental test.

Parameter	Symbol	Unit	Value
Journal diameter	D	m	0.05
Bearing length	L	m	0.0498
Radial clearance	c	m	0.0001
Rotational speed	N	rpm	3600
Lubrication viscosity at 40°c (155 Diesel oil)	μ	Pa . s	0.1793
Lubrication viscosity at 100°c (155 Diesel oil)	μ	Pa . s	0.0169
Lubrication density	ρ	Kg/m ³	902.1

Table (5-2) The journal bearing characteristic of the case study

Parameter	Symbol	Unit	Value
Journal diameter	D	m	0.05
Bearing length	L	m	0.025
Radial clearance	c	m	0.000025
Rotational speed	N	rpm	4000
Lubrication viscosity[2]	μ	Pa .s	0.00416
eccentricity ratio	ε	–	0.58

5.1 Experimental Results

The results of the experimental work are shown in the table (5-3) and figure (5-1).

From this figure it can be concluded that the maximum oil film pressure is (3.6084 kPa) at angle 90 deg., measured from the oil inlet. This results were compare with numerical results illustrated in figure (5-2) and (5-3). Since it is difficult to determine, measure or calculate the value of eccentricity ratio experimentally. So for the sake of comparison with the numerical results a wide range of eccentricity ratio (0.01-0.7) covering the actual ratio of eccentricity ratio are taken as shown in figures (5-2) and (5-3). From these figures it can be deduced that the maximum pressure increases as the eccentricity ratio increases.

Since the maximum pressure in the lowest value of the eccentricity ratio (0.01) is (11.831 kPa) which is higher the experimental results, this leads to the fact that the experimental results can not be depended for the comparisin.

The high error in the measuring the pressure distrbution expermentaly is attributed to the side leakage of the lubricant. The side leakage is mainly caused by the missalignment of the journal. The missalignment test needs high precession tachnologue which is very expensive and not availble in iraqi industry companies.

Hence the experiment work can not be valid in comparison with the dynamic cases.

Table (5-3) The expermental results

Angle location (deg.)	Pressure (kPa)	Temperature (C)
0	0.09021	91.3
90	3.6084	89.9
112.5	0.09021	90
135	0	90.8
157.5	0	89.2
180	0	90.3
202.5	0	89.5
225	0	90.4
247.5	0	90
270	1.62378	90.5
360	0.09021	91.3

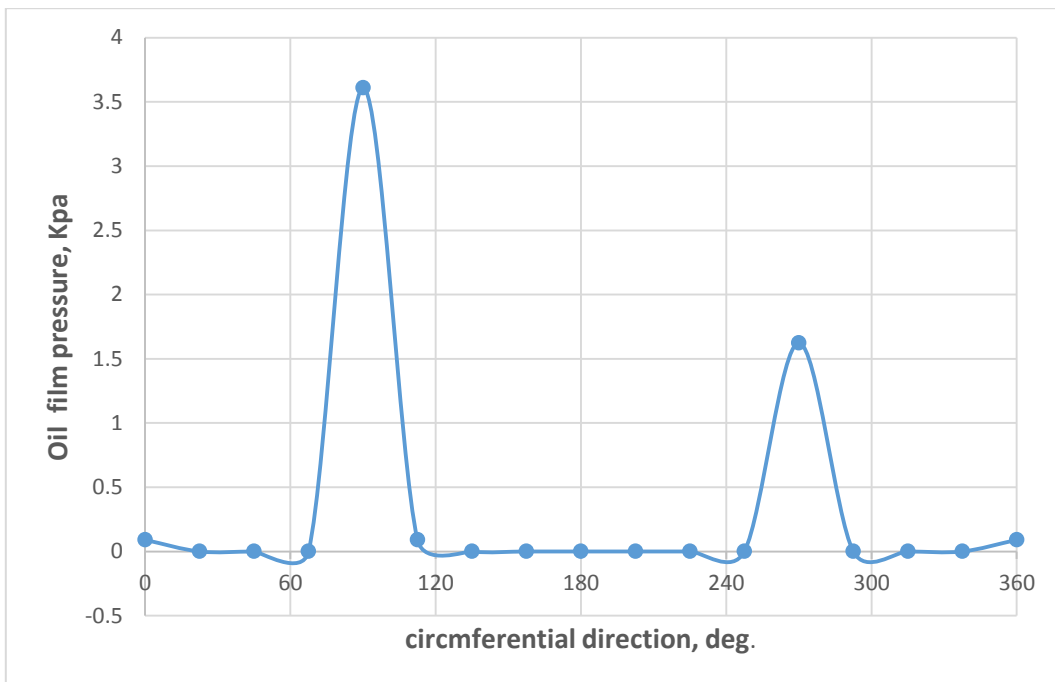


Figure (5-1) The oil film Pressure obtained from the experimental test

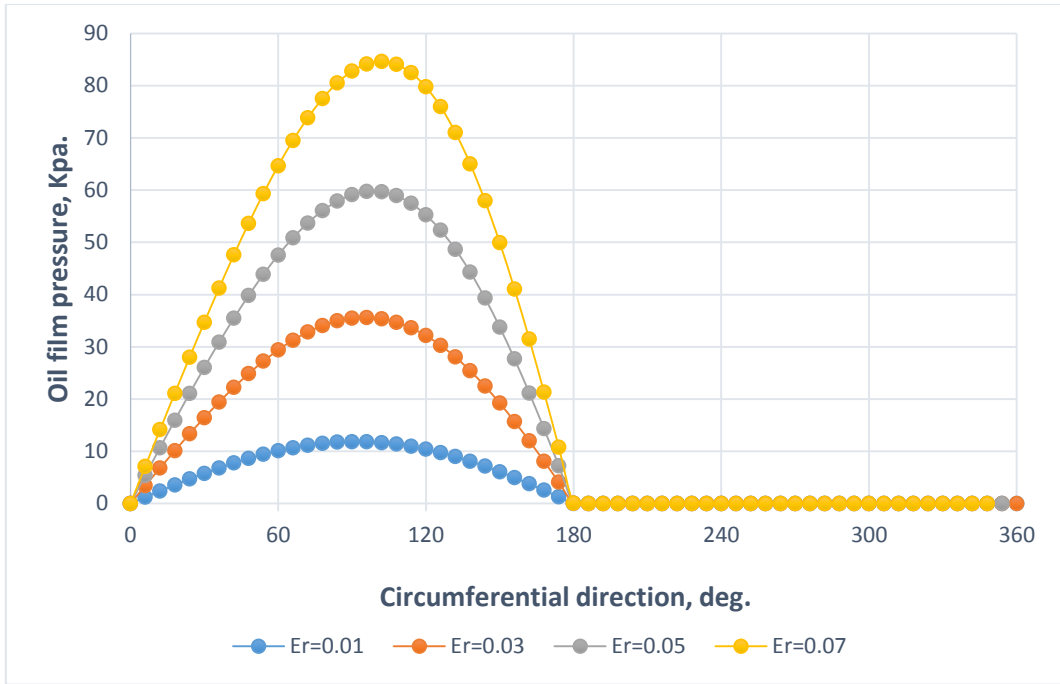


Figure (5-2) Numerical oil film pressure distribution of different values of eccentricity ratio up to 0.07.

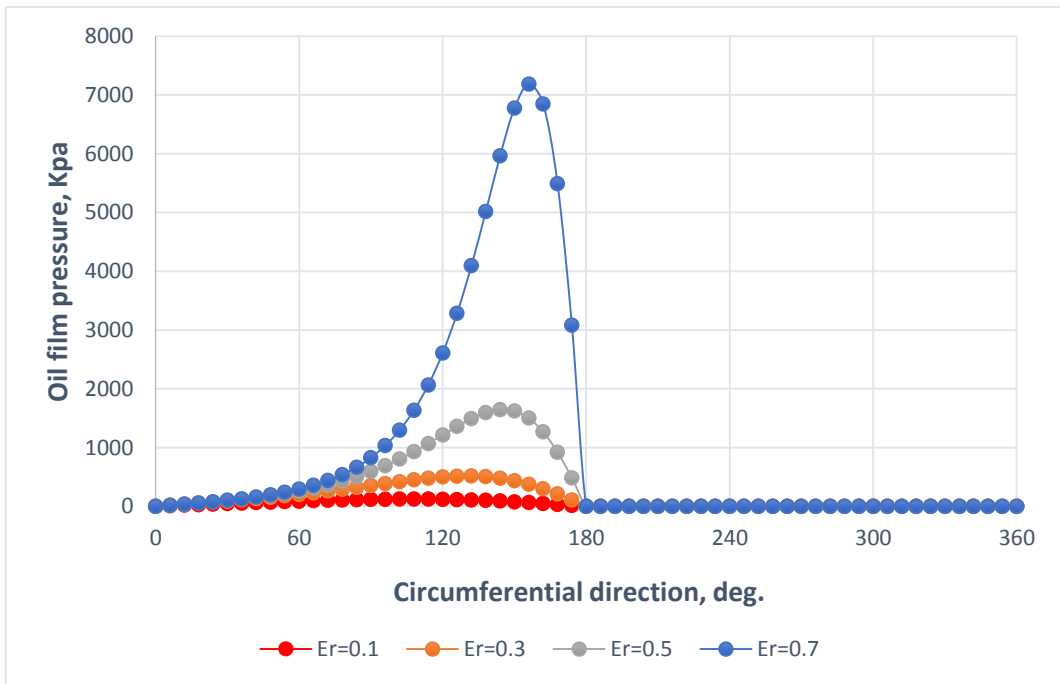


Figure (5-3) Numerical oil film pressure distribution of different values of eccentricity ratio up to 0.7

5.2 Numerical results

In this section the results of solving the Reynold equation numerically are discussed in both steady state and dynamic case using the data listed in table (5-2).

5.2.1 Convergence steady

The size of the mesh in solving the Reynolds equation play an important part in the accuracy of the results.

So a convergence study is very important to determine the size of mesh adopted.

In this thesis nine types of mesh are tested to select the best one from the accuracy and execution time points of views

Table (5-4) Convergence criteria

Mesh size (n × m)	MAX. Pressure (mPa)
11×11	2.78746
21×13	2.93091
31×15	2.95794
41×17	3.03742
51×19	3.06294
61×21	3.06851
71×23	3.06723
81×25	3.06355

So to ensure accurate results with minimum CPU time, the mesh size of (61 ×21) nodes is chosen in θ and z directions, respectively.

5.2.3 Steady state results

The effects of different values of eccentricity ratio on the oil film pressure and oil film thickness for the same rotational speed, lubricant viscosity and same aspect ratio (as listed in table 5-2) are illustrated in figures (5-4) and (5-5) respectively.

When the eccentricity ratio increases the maximum oil film pressure increases while the oil film thickness decreases so that the gap between the shaft and the bearing decreases.

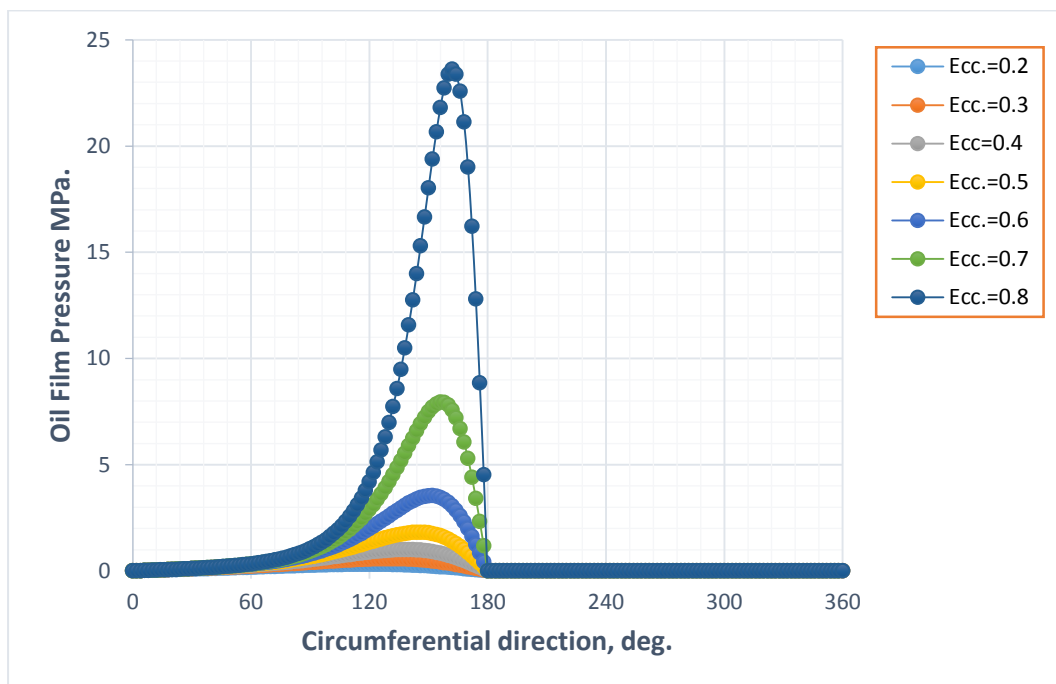


Figure (5-4) Oil film Pressure distribution at different values of eccentricity ratio

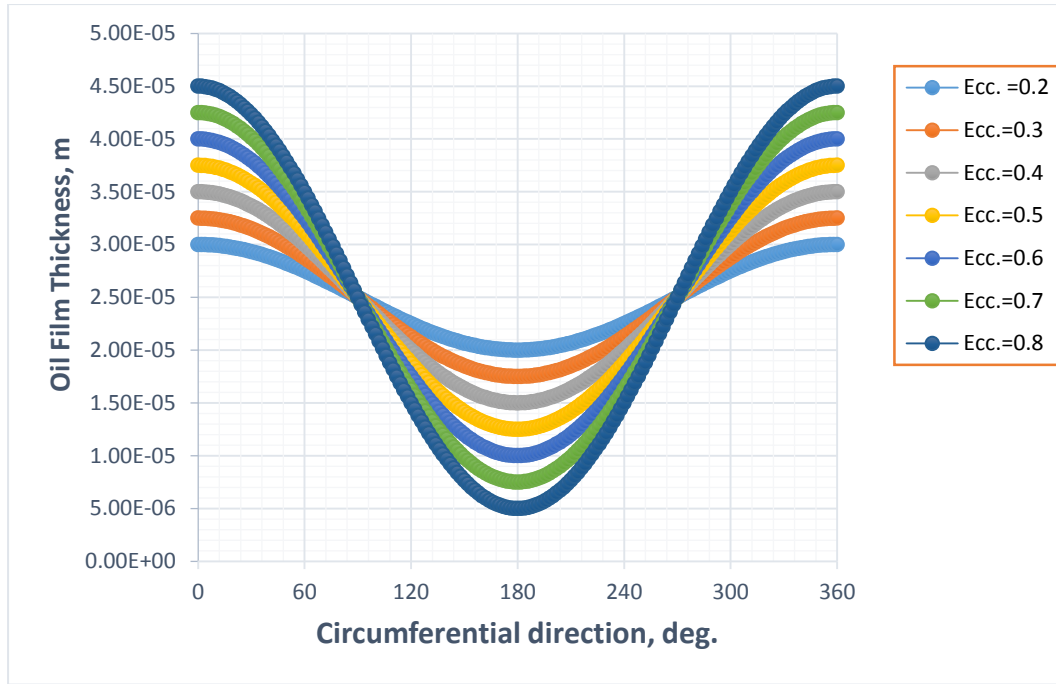


Figure (5-5) Oil film thickness at different values of eccentricity ratio

The effect of the rotational speed on the maximum oil film pressure for different value of eccentricity ratio is illustrated in figure (5-6).

It is clearly noticed that increasing the rotational speed leads to the increasing in the maximum oil film pressure due to increasing in hydrodynamic effect.

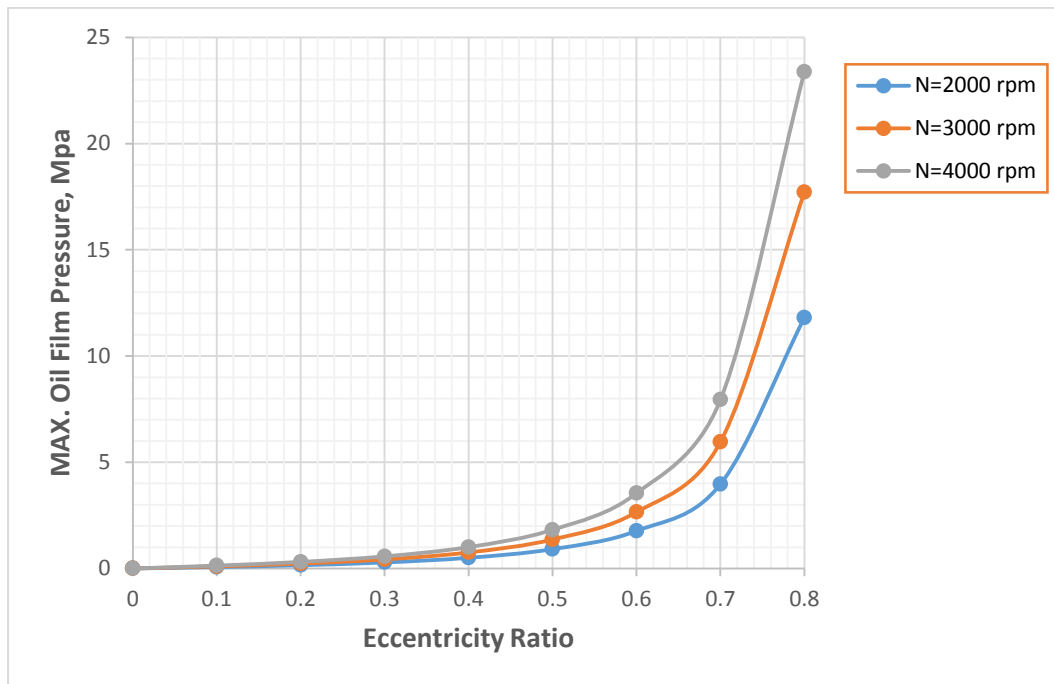


Figure (5-6) Maximum oil film pressure versus eccentricity ratio for different values of rotational speed

The effect of aspect ratio on the oil film pressure distribution with all other parameters are fixed as listed in table (5-2), is illustrated in the figure (5-7).

It can be found that for large value of aspect ratio (L/D) the pressure increases. This is attributed to the fact that when the length of bearing increases, the effect of side leakage decreases causing the pressure to be increase.

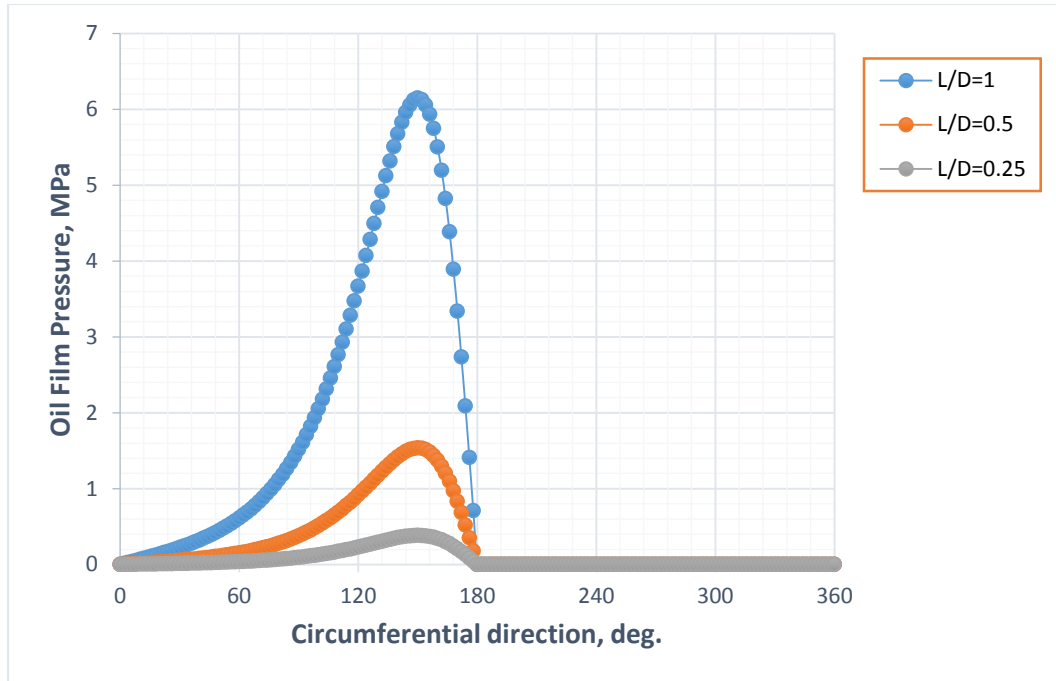


Figure (5-7) Oil film Pressure at different values of aspect ratio

The effect of eccentricity ratio on the load carrying capacity is illustrated in figure (5-8). It can be found that the more values of eccentricity ratio, the more load carrying capacity resulted.

This results is expected to occur because the load carrying capacity increases as the oil film pressure increases.

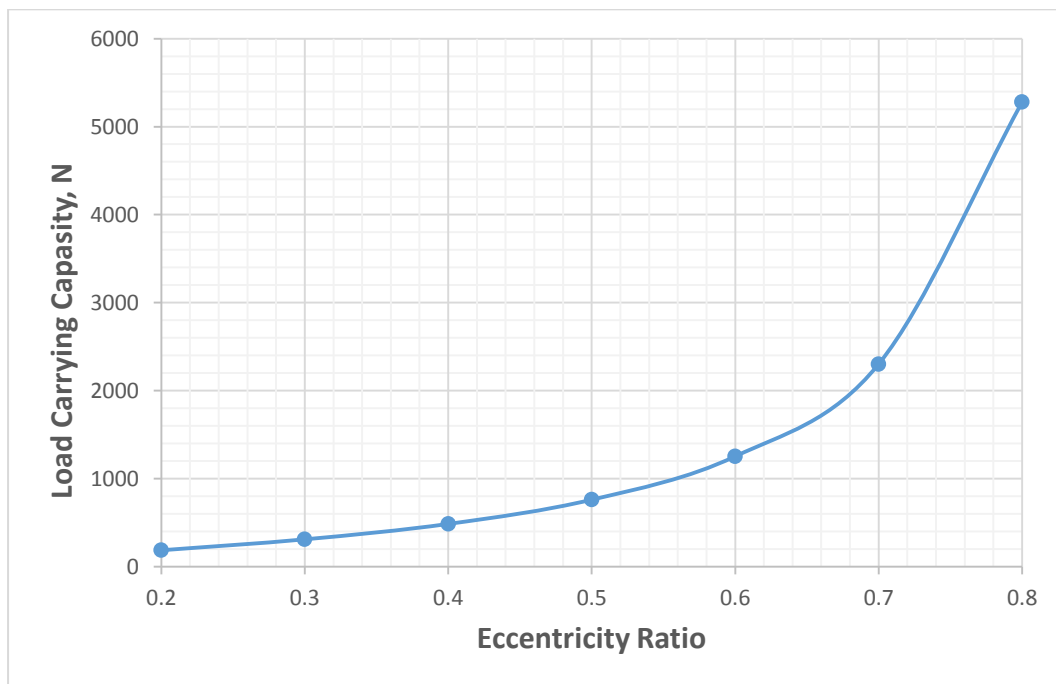


Figure (5-8) Load carrying capacity versus eccentricity ratio.

The effect of the rotational speed on the load carrying capacity for different value of aspect ratio is illustrated in figure (5-9). It can be noticed that the load carrying capacity is enhanced with the increasing of rotational speed of the shaft for higher length to diameter ratio due to the increasing in oil film pressure as discussed.

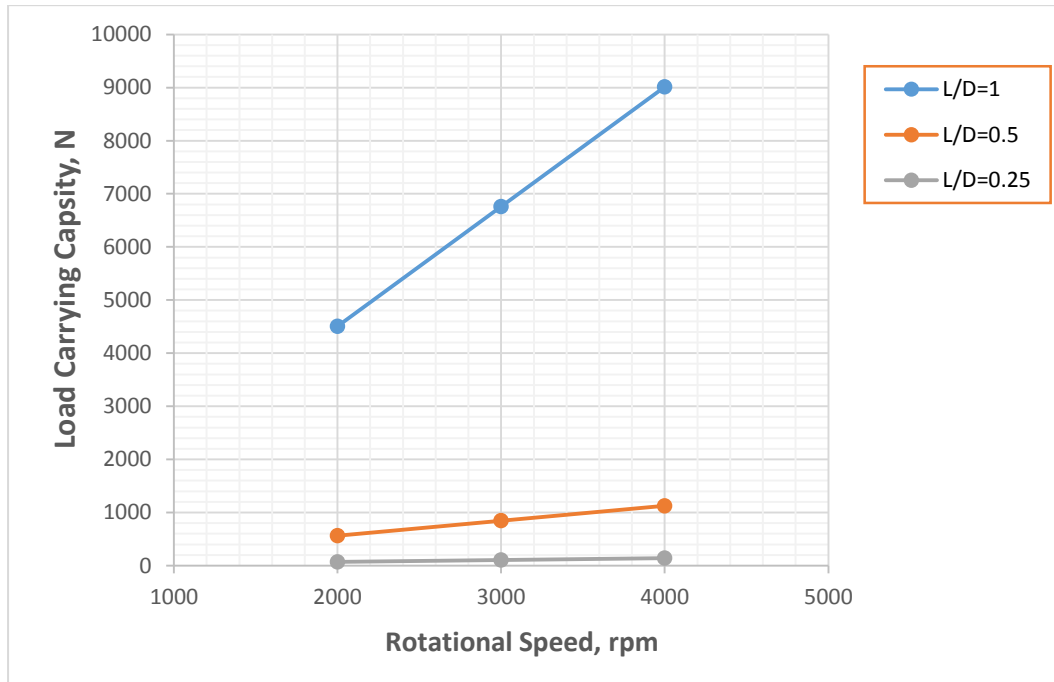


Figure (5-9) Load carrying capacity versus rotational speed for different value of aspect ratios.

Figure (5-10) and (5-11) show the behavior of the oil film pressure and thickness in three dimension. It is observed that the maximum oil film - pressure locates at the central plan of bearing length while the oil film thickness is constant in the axial direction. Also these figures show that the location of the maximum pressure in the circumferential direction coincides approximately of that minimum film thickness.

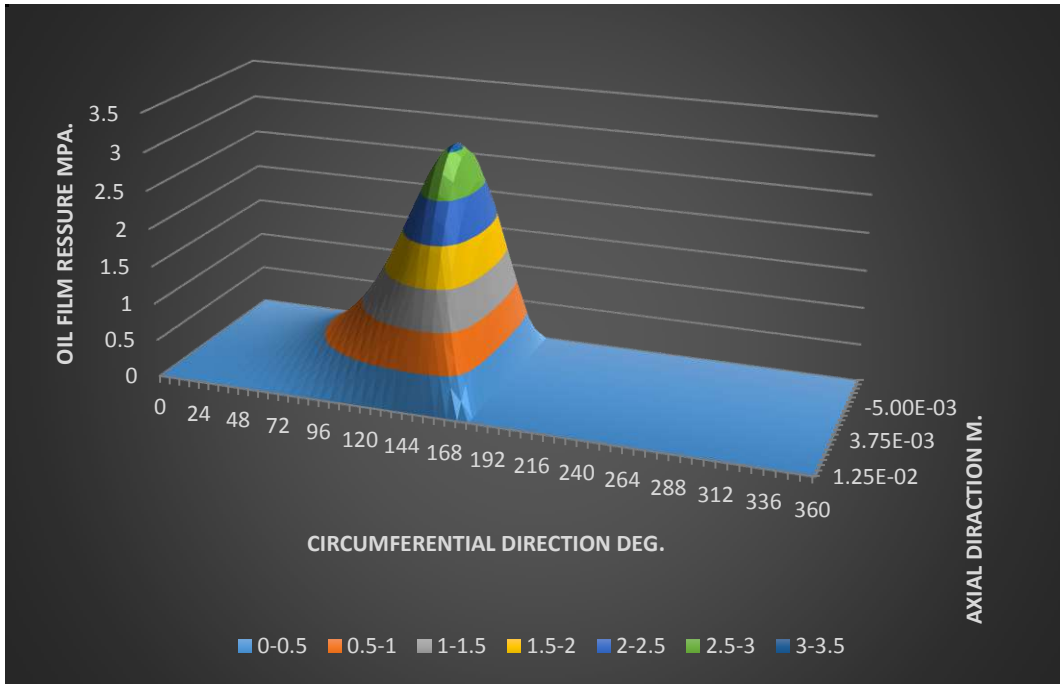


Figure (5-10) 3-D Oil film pressure distribution along the circumferential direction of journal bearing

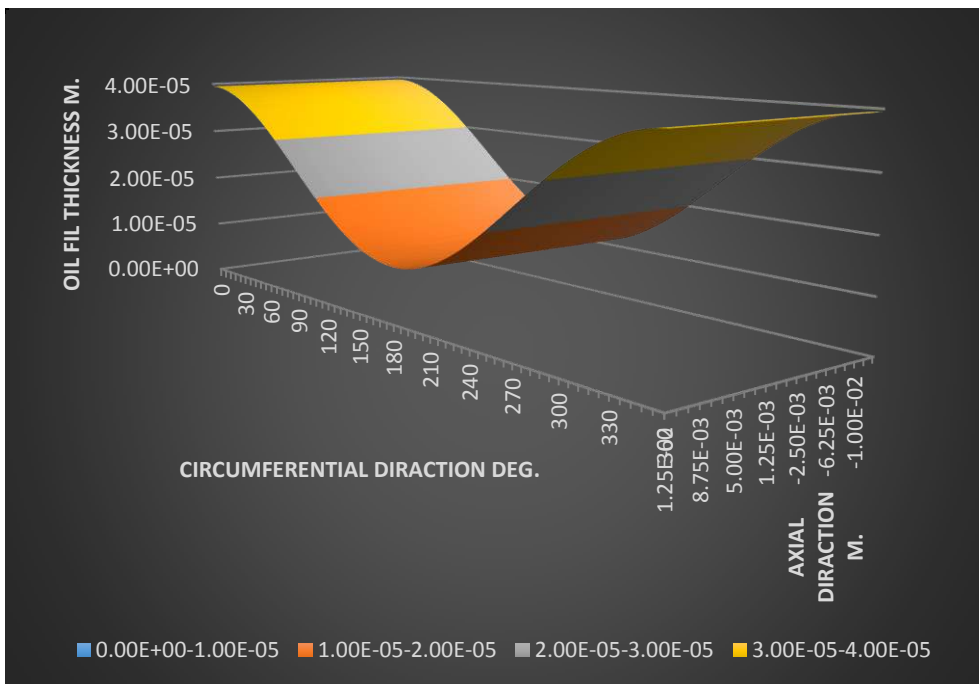


Figure (5-11) 3-D Oil film thickness distribution along the circumferential direction of journal bearing

5.2.4 Dynamically loaded results

5.2.4.1 The effect of self excited vibration only

Figure (5-12) shows the velocity of the journal locus during a short period of time for different value of attitude angle. It can be observed that the velocity distribution changes for $\varphi = 2.5$ rad and 3.5 rad. Also it can be observed that for higher φ the velocity of the journal center increases. These observations can be attributed to the fact of sign of $(\cos \varphi)$ in equation (3.36).

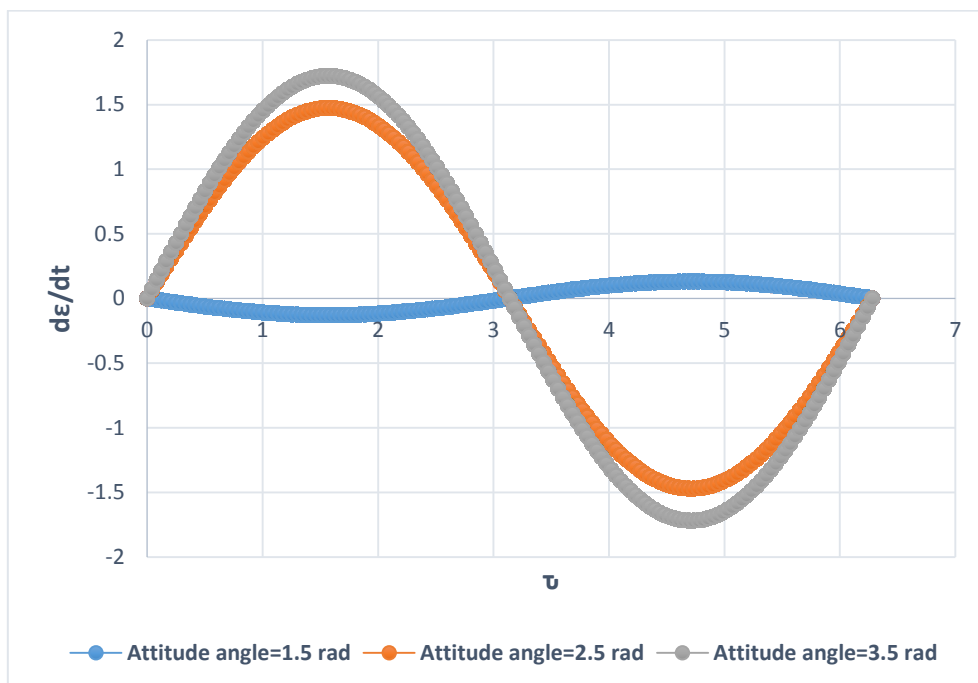


Figure (5-12) The velocity of the center of journal versus the non-dimensional response time for different values of φ under a sinusoidal load

Figure (5-13) shows the velocity of the journal locus relation with the time period for different values of eccentricity ratio under a cyclic loading. It is clear that for higher eccentricity ratio the velocity of the journal center decreases. This trend is due to the term of $(1 - \varepsilon^2)$ in the

numerator and the term of $(1 + 2\epsilon^2)$ in the denomantor in equation (3.36).

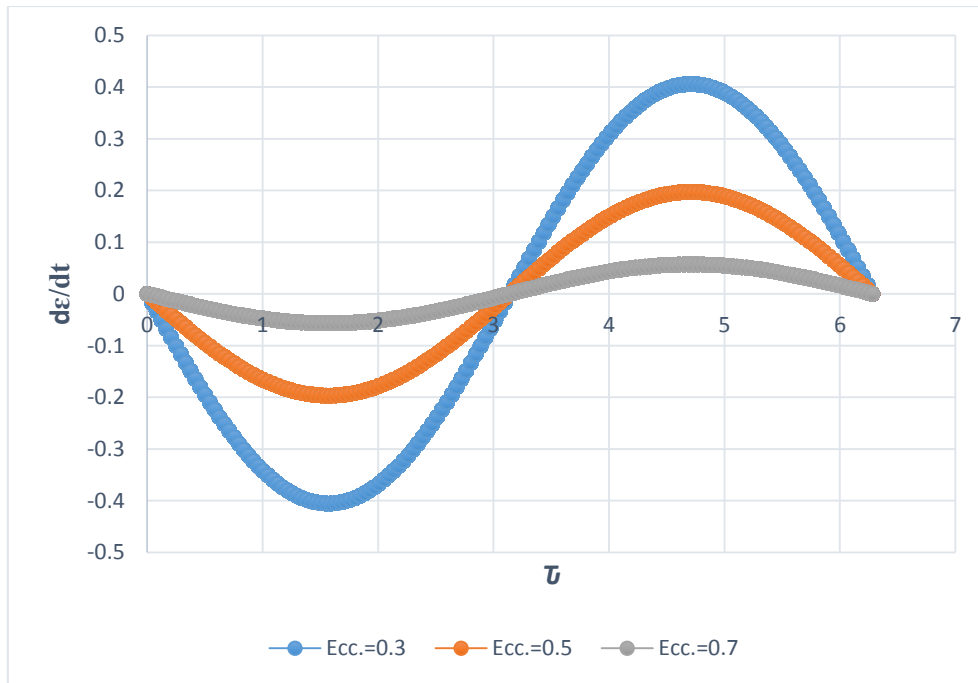


Figure (5-13) The velocity of the center of journal versus the non-dimensional response time for different values of ϵ under a sinusoidal load

Figure (5-14) Shows the oil film pressure distributiona long the circumferntial direction for different values of eccentricity ratio. It is found that the oil film pressure is affected gearatly with the increasing of eccentricity ratio. This trend agrees with that of the study state case. Furthermore it can be observed that the location of the maximum is shafted towerd the inlet of oil as the eccentricity ratio increases.

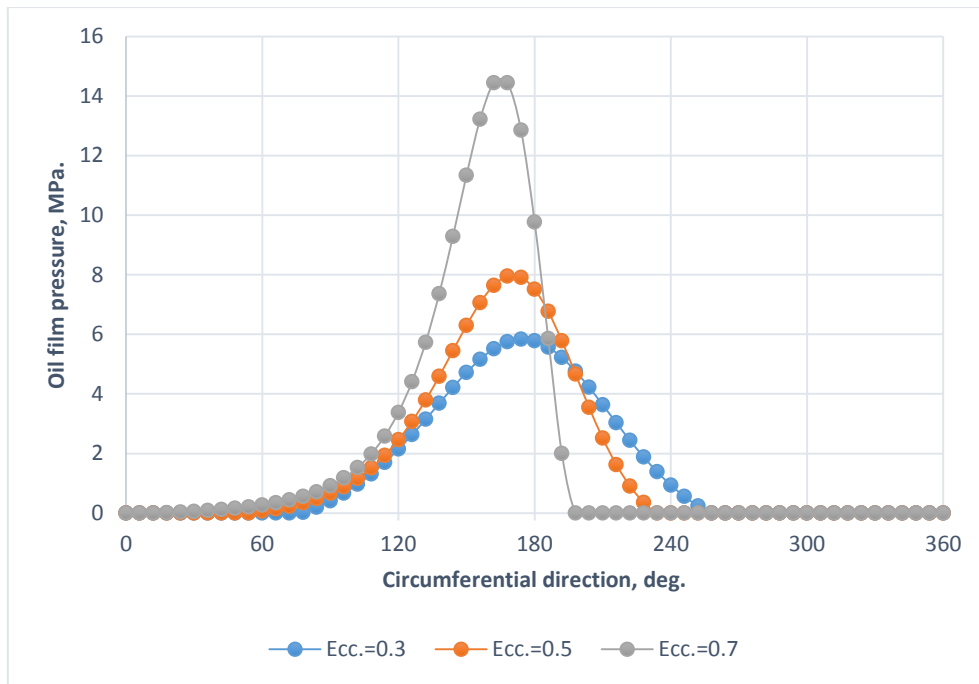


Figure (5-14) Oil film Pressure versus the circumferential direction for different values of ϵ

Figure (5-15) shows the oil film pressure distribution along the circumferential direction for different values of attitude angle under a cyclic loading. It is found that the increasing in the attitude angle causes increasing in the oil film pressure. It is also noticed that the pressure distribution exhibits the same behavior for a various value of attitude angle. This is due to the fact the increasing of φ leads to increase ϵ which result the oil pressure to be increased.

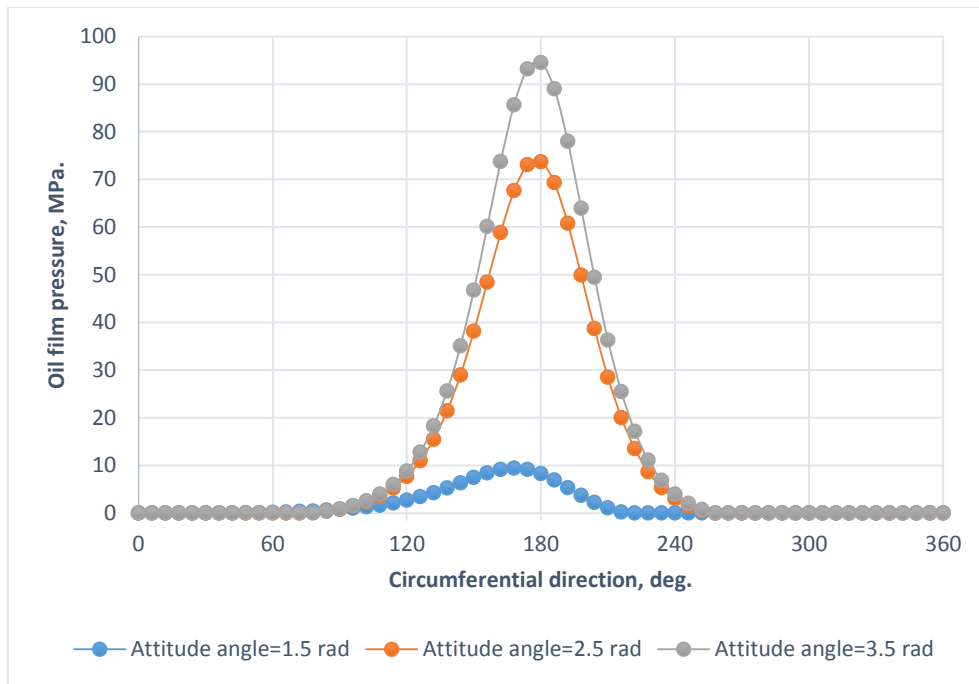


Figure (5-15) Oil film Pressure distribution along the circumferential direction for different values of φ

Figure (5-16) shows that the load carrying capacity increases with increasing of eccentricity ratio and the rotational speed. This behavior agrees with that of in the steady state case.

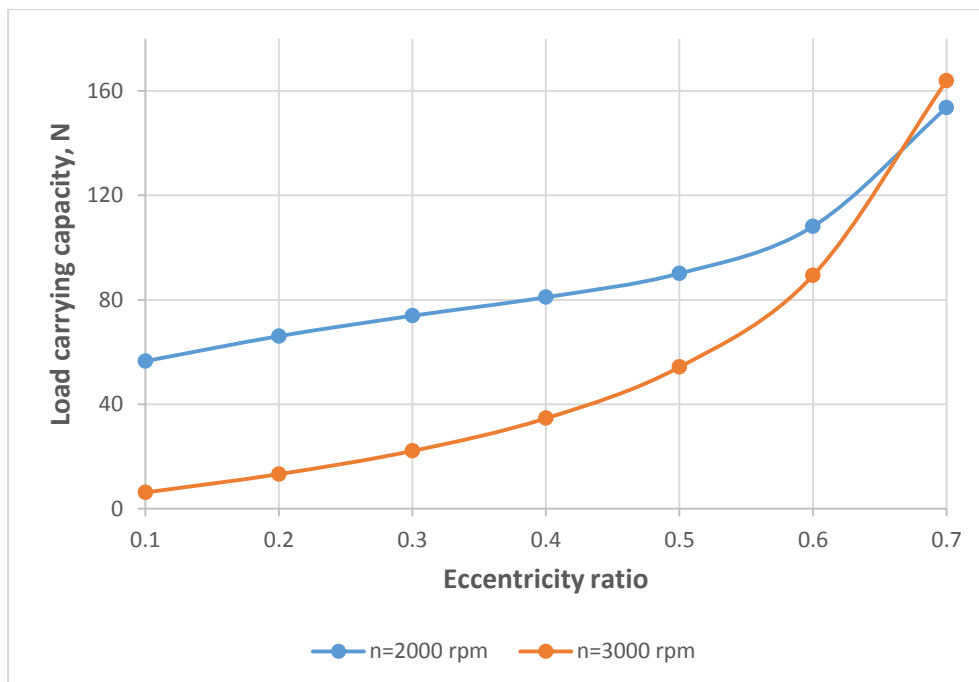


Figure (5-16) Load carrying capacity versus eccentricity ratio for different values of rotational speeds.

Figure (5-17) shows the oil film pressure distribution under the effect of self-excited vibration in three dimension. It is found that the maximum oil film pressure obtained is (9.423 MPa). It can be observed the maximum value of the oil film pressure is occurred at ($\theta = 168$ deg.).

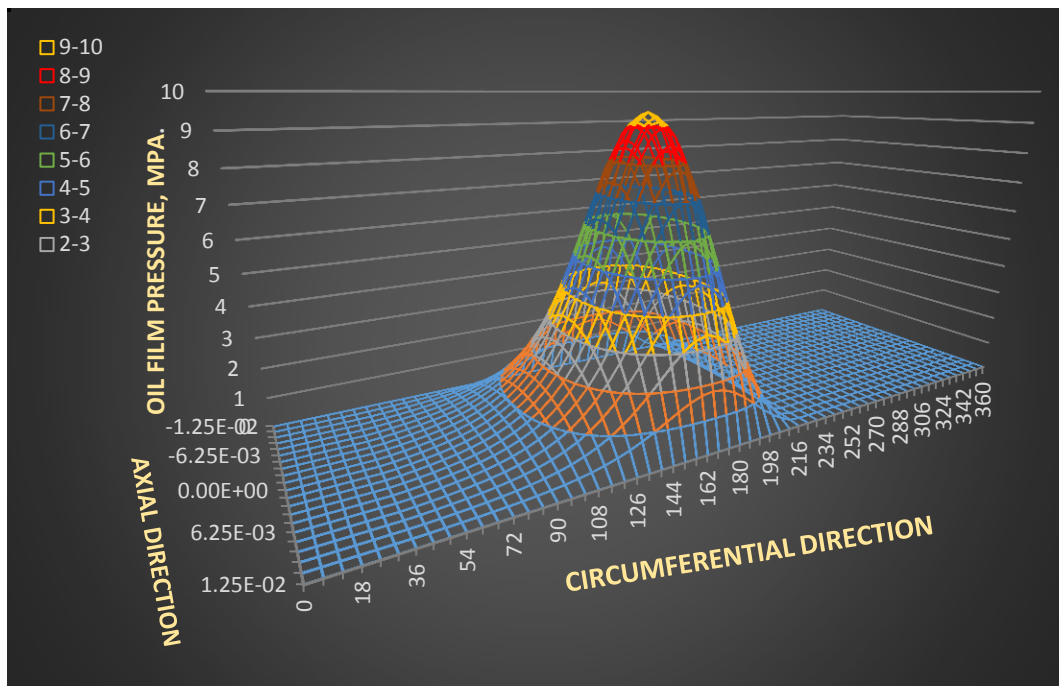


Figure (5-17) Oil film Pressure distribution along the circumferential direction of journal bearing in 3- dimension.

5.2.4.2 The effect of forced harmonic excitation only

Figure (5-18) shows the oil film pressure distribution with the circumferential direction for different values of the amplitude of the force which causes the system to vibrate. The increasing of the amplitude of the force increases the oil film pressure. This is due to the fact that increasing of the external force on the bearing system causes the gap between the bearing and journal to be decreased causing to increase the oil film pressure.

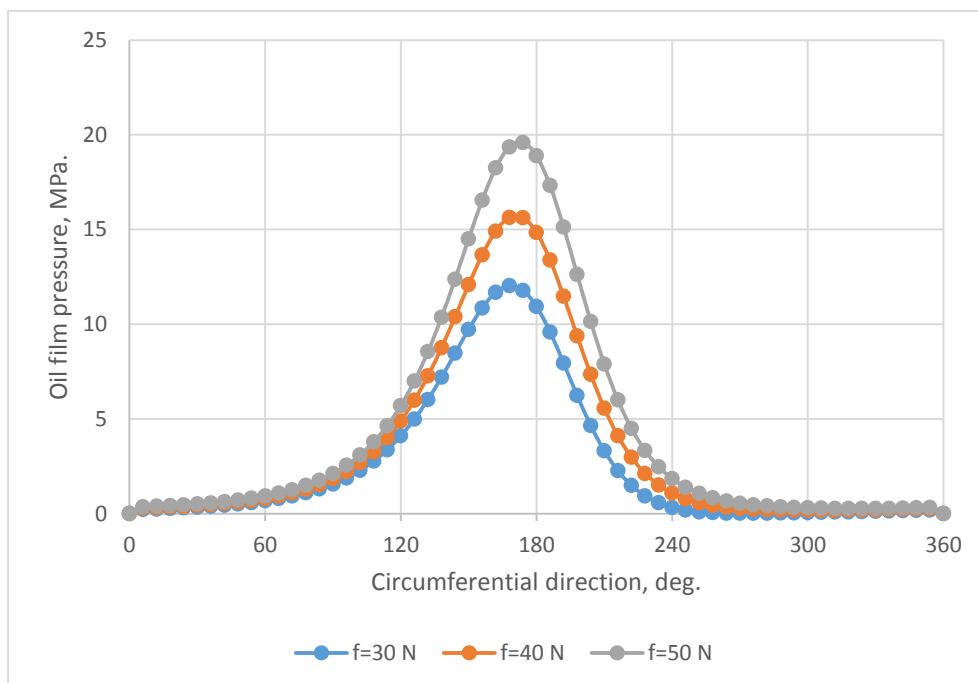


Figure (5-18) Oil film Pressure at different values of amplitude of forced vibration

Figure (5-19) shows the maximum oil film pressure during one second for a different value of damping ratio at the same value of the amplitude of vibration force which equals to (20 N). It is observed that the increasing the damping ratio causes a reduction in the oil film pressure. This is due to the fact that the damping dissipates the energy of vibration and then decreases the amplitude of vibration response.

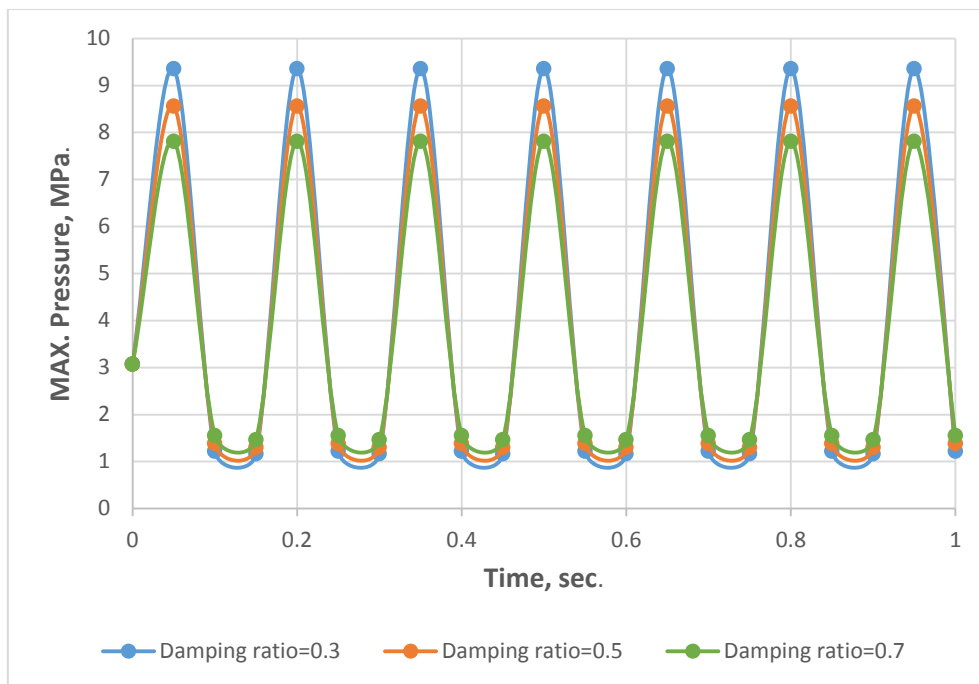


Figure (5-19) Maximum oil film pressure versus time for different values of damping ratio.

Figure (5-20) shows the minimum oil film thickness verse damping factor for different value of ω/ω_n under the effect of external forced harmonic vibration. It is observed that the minimum oil film thickness increases with the increases of frequency ratio. Hence that is led to decreases the oil film pressure.

Also it is observed that for higher frequency ratio, increasing the damping ratio has no considerable effect on the minimum film thickness.

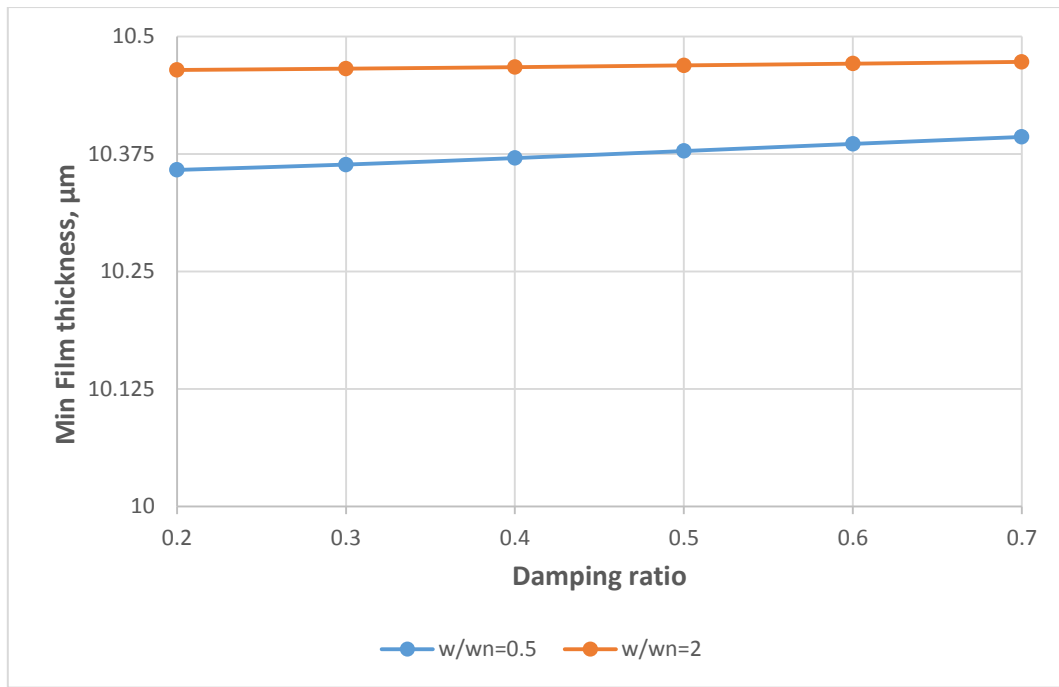


Figure (5-20) Minimum film thickness versus damping ratio for different values of (ω/ω_n) .

Figure (5-21) shows the distribution of oil film pressure along the circumferential direction for different ratios of ω/ω_n . It found that the higher frequency ratio, the lower oil film pressure resulted. This attributed to the fact that the increasing the frequency ratio leads to increase the minimum oil film thickness causing the oil film pressure to be decreased.

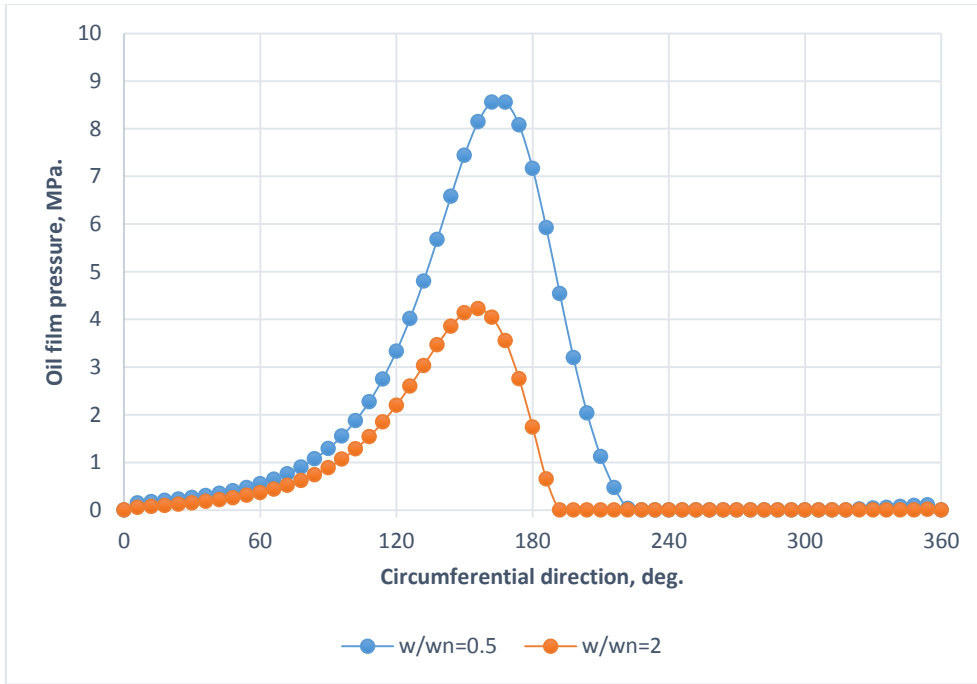


Figure (5-21) Oil film pressure distribution for different values (ω/ω_n)

Figure (5-22) shows the oil film pressure distribution under the effect of external forced harmonic excitation in three dimension. It is found that the maximum oil film pressure obtained is (19.601 MPa) and it located at ($\theta = 174$ deg.).

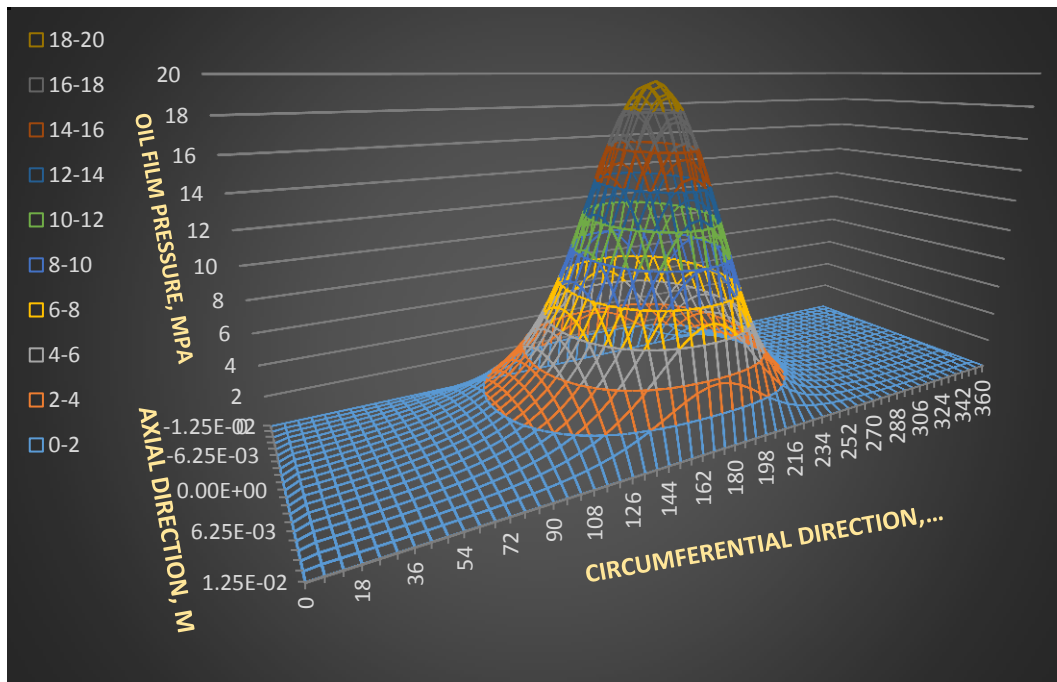


Figure (5-22) Oil film Pressure distribution along the circumferential direction of journal bearing in 3- dimension

5.2.4.3 The combined effect of the self excited and external forced harmonic vibration.

Figure (5-23) shows the maximum oil film pressure of dynamically loaded with and without the effect of forced vibration as a function of time. It is observed that the maximum oil film pressure increases in the case of the combined effect. The percentage of this increment is 36.662 % . The fluctuating trend is attributed to the sinusoidal nature of load in the harmonic excitation.

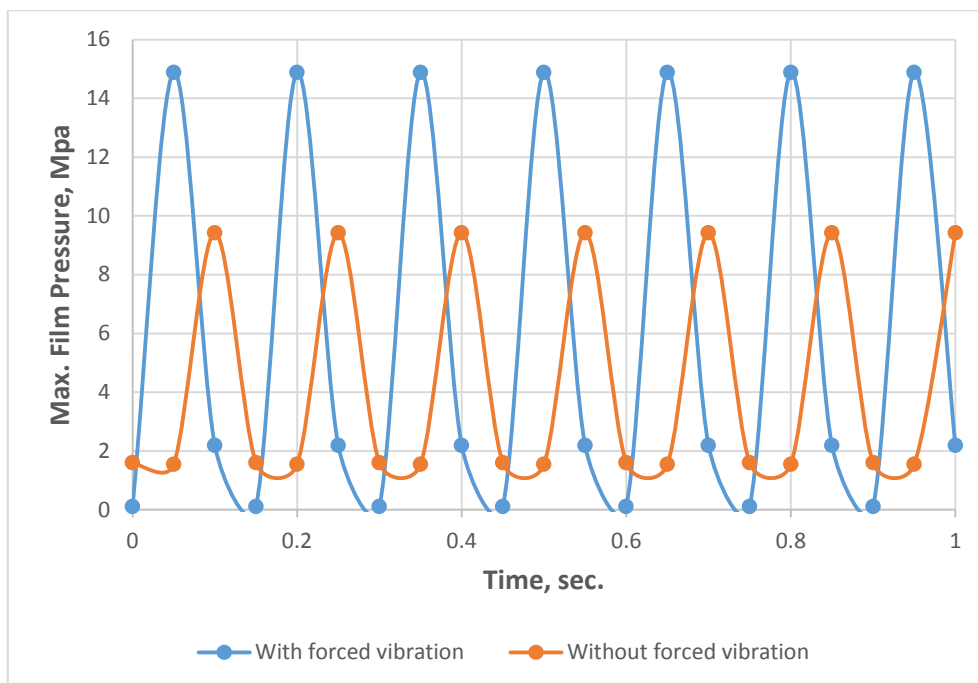


Figure (5-23) Maximum pressure distribution of the journal bearing with and without forced vibration effect during 1 sec

Figure (5-24) shows the distribution of oil film pressure during a certain time along the circumferential direction. It is found that the increasing in the amplitude of the vibration force causes the pressure to increase.

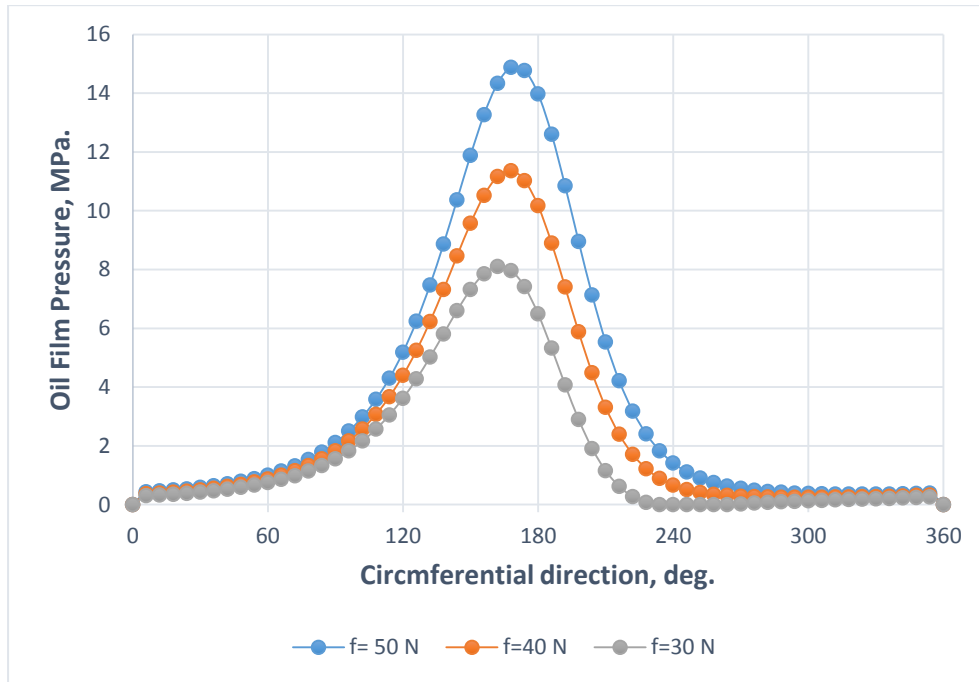


Figure (5-24) Oil film Pressure for different values of amplitude of forced vibration

Figure (5-25), shows the variation of the maximum oil film pressure with the damping ratio for different value of ω/ω_n ratio.

It observed that for $\frac{\omega}{\omega_n} < 1$, the maximum oil film pressure decreases significantly with the damping ratio. While for $\frac{\omega}{\omega_n} > 1$, the effect of the damping ratio on the maximum oil film pressure is little.

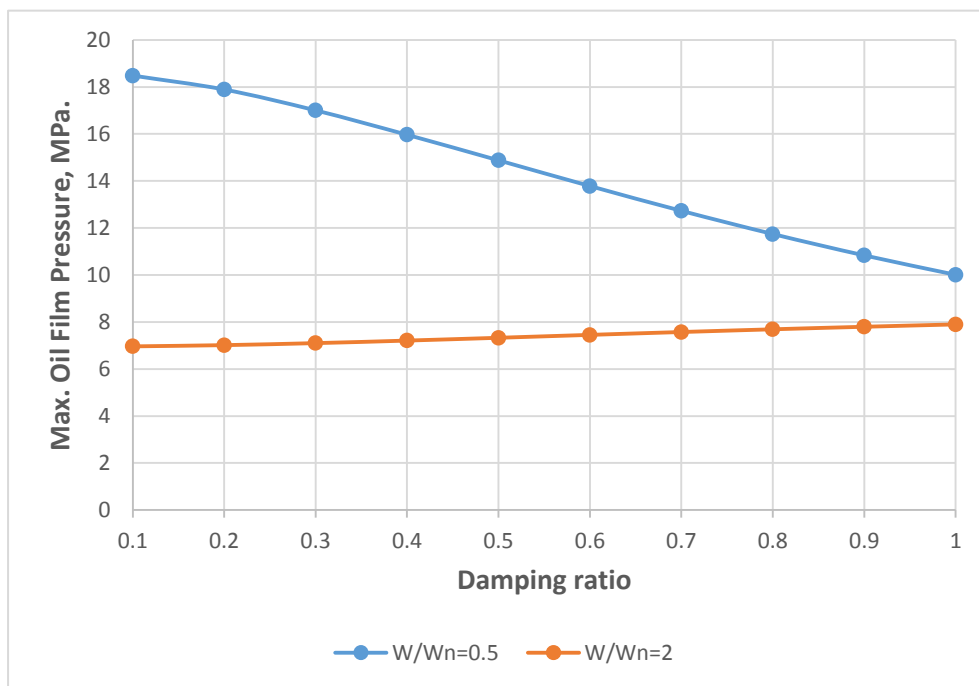


Figure (5-25) Maximum pressure distribution versus damping ratio for different values of (ω/ω_n) .

Figure (5-26) and table (5-5) show the variation of the maximum oil film pressure with time for different value of damping ratio. It can be concluded that as the damping ratio increases the maximum pressure decreases. This trained is the same as seen in the case of the effect of external vibration only.

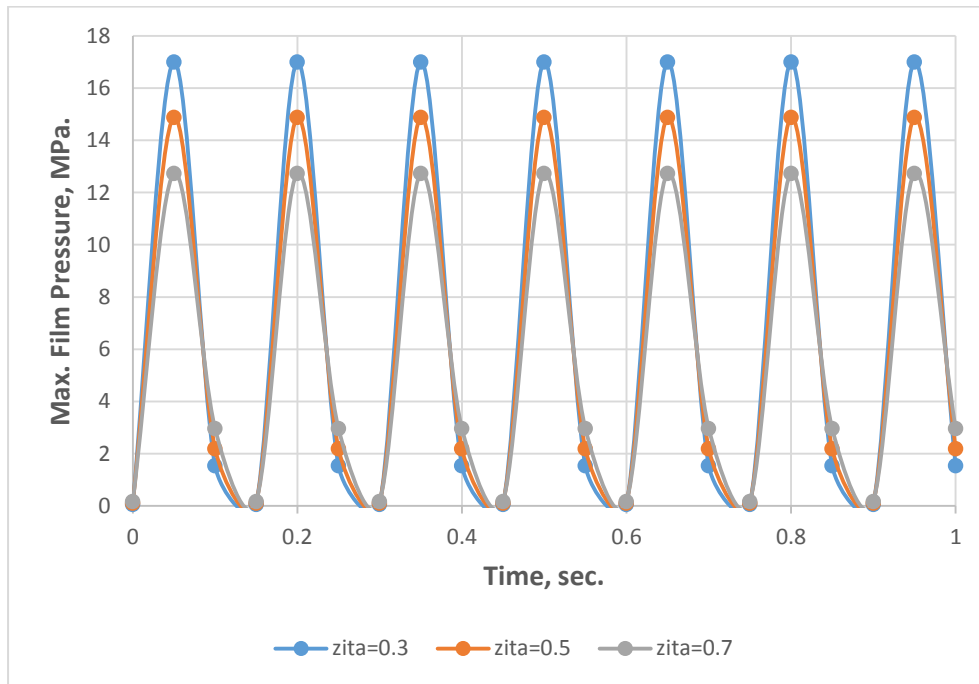


Figure (5-26) Maximum oil film pressure for different values of damping ratio during 1 sec.

Table (5-5) Maximum oil film pressure for different values of damping ratio

Time (sec)	$\xi = 0.3$ Max. Pressure(MPa)	$\xi = 0.5$ Max. Pressure(MPa)	$\xi = 0.7$ Max. Pressure(MPa)
0	0.053194	0.105857	0.174833
0.05	17.002	14.8777	12.7293
0.1	1.54238	2.19066	2.96627
0.15	0.053198	0.105856	0.174833
0.2	17.002	14.8777	12.7293
0.25	1.54236	2.19063	2.96626
0.3	0.053198	0.105856	0.174836
0.35	17.002	14.8777	12.7293
0.4	1.54234	2.19062	2.96624
0.45	0.053202	0.105861	0.174836
0.5	17.0021	14.8778	12.7294
0.55	1.54233	2.19059	2.96623
0.6	0.053202	0.105866	0.17484
0.65	17.0021	14.8778	12.7294
0.7	1.54228	2.19058	2.96621
0.75	0.053207	0.105866	0.17484
0.8	17.0021	14.8778	12.7294
0.85	1.54227	2.19055	2.96618
0.9	0.053207	0.105866	0.17484
0.95	17.0021	14.8778	12.7294
1	1.54225	2.19054	2.96616

Figure (5-27) and table (5-6) shows the variation of maximum pressure with time for different value of frequency ratio. It is can be noticed that for higher frequency ratio the maximum pressure decreases. While for a low frequency ratio, the maximum pressure increases. This trend and the sinusoidal fluctuation are the same as seen in the case of external forced vibration only.

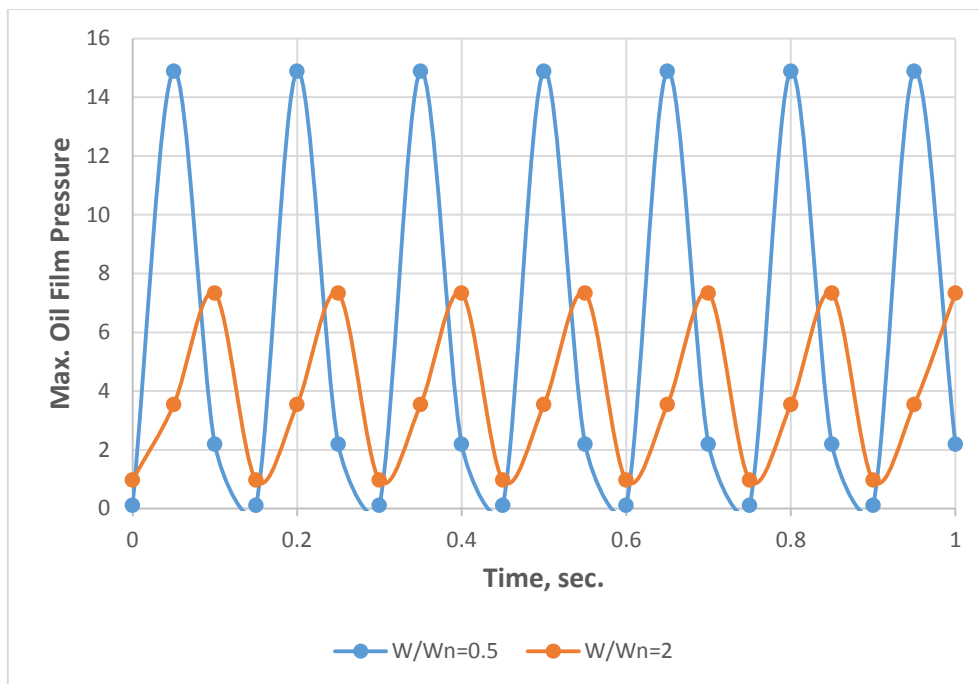


Figure (5-26) Maximum oil film pressure distribution for different values (ω/ω_n) during 1 sec.

Table (5-6) Maximum oil film pressure distribution for different values (ω/ω_n)

Time (sec)	$\omega/\omega_n = 0.5$	$\omega/\omega_n = 2$
	Max. Pressure(MPa)	Max. Pressure(MPa)
0	0.105857	0.970501
0.05	14.8777	3.5333
0.1	2.19066	7.32873
0.15	0.105856	0.970508
0.2	14.8777	3.53331
0.25	2.19063	7.32873
0.3	0.105856	0.970508
0.35	14.8777	3.53331
0.4	2.19062	7.32873
0.45	0.105861	0.970512
0.5	14.8778	3.53331
0.55	2.19059	7.32873
0.6	0.105866	0.970512
0.65	14.8778	3.53334
0.7	2.19058	7.32873
0.75	0.105866	0.970512
0.8	14.8778	3.53334
0.85	2.19055	7.3287
0.9	0.105866	0.970512
0.95	14.8778	3.53334
1	2.19054	7.3287

Figure (5-28) shows the maximum oil film pressure and minimum film thickness as a function of time. A little change in oil film thickness causes a significant variation in the film pressure. Also it can be noticed that a sinusoidal fluctuation in the oil film thickness occurs as founded in the oil film pressure

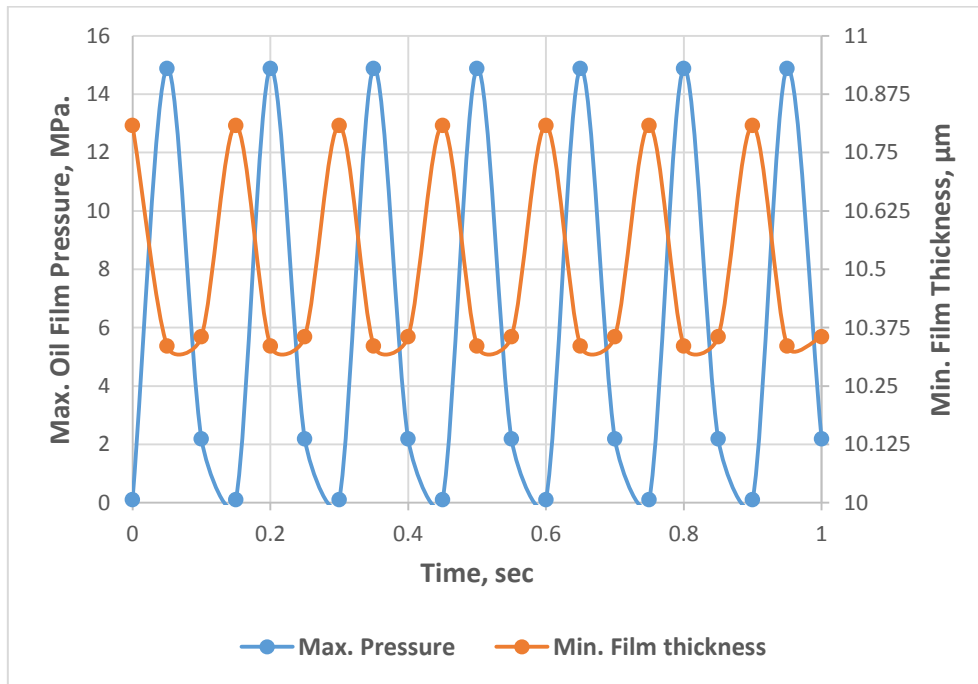


Figure (5-28) Maximum oil film pressure and minimum film thickness variation during 1 sec.

Figure (5-29) shows the minimum film thickness versus damping ratio for different values of ω/ω_n . It is observed that for higher frequency ratio, increasing the damping ratio has no considerable effect on the minimum film thickness. While for low frequency ratio, the minimum oil film thickness increases considerably with the increases of damping factor leading to decreases the oil film pressure.

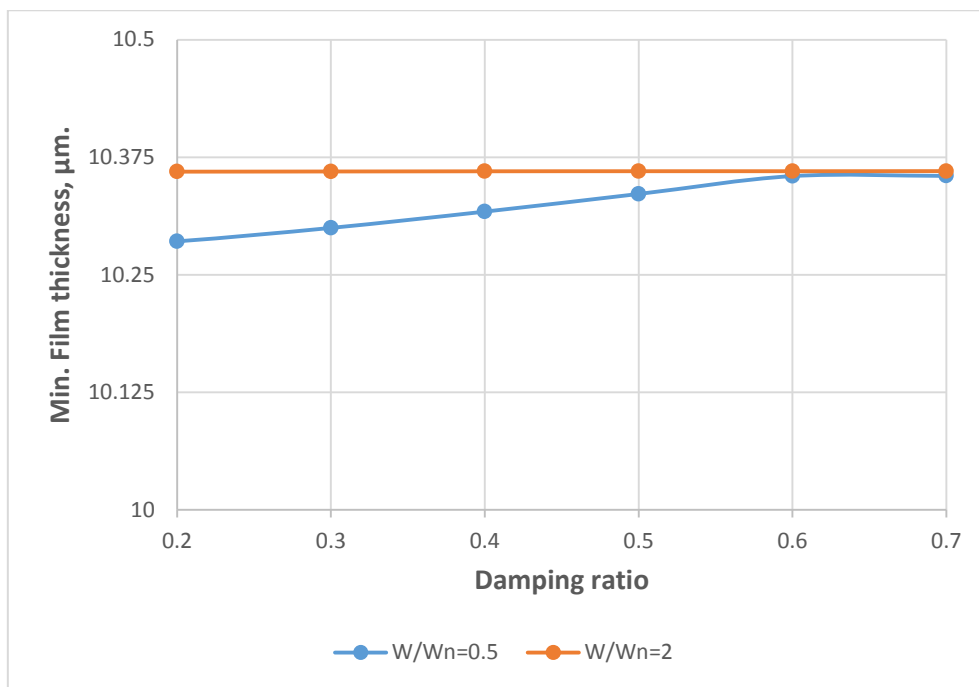


Figure (5-29) Minimum film thickness versus damping ratio for different values of (ω/ω_n) .

Figure (5-30) shows the oil film pressure distribution under the combine effect of self-excited vibration and forced harmonic excitation in three dimension. It can be observed the maximum value of the oil film pressure is occurred at ($\theta = 168$ deg.). While the corresponding positions in both the steady state, self-excitation and external forced harmonic cases are (144, 168, 174) respectively. That means the location of the maximum oil film pressure is shifted to the exit of the oil in the dynamic cases.

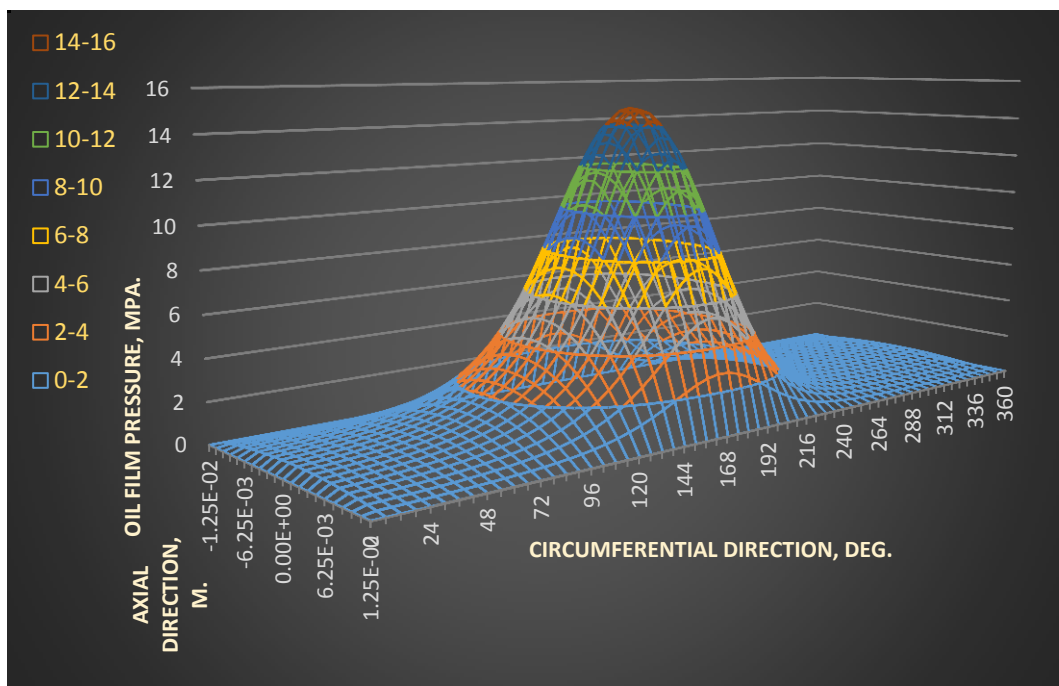


Figure (5-30) Oil film Pressure distribution along the circumferential direction of journal bearing in 3- dimension.

CONCLUSION AND RECOMMENDATIONS

6.1 The conclusions

From the preceding chapters of this thesis, the following conclusions can be withdrawn:

1. The maximum oil film pressure is increased under the effect of the combine case compared to the effect of self-exited only by (36.66 %).
2. The oil film pressure is increased as the amplitude of vibration force increases
3. The oil film pressure is decreased for large value of damping ratio up to 0.7
4. The oil film pressure decreases for $(\frac{\omega}{\omega_n} > 1)$, while increases for $(\frac{\omega}{\omega_n} < 1)$.
5. The location of maximum oil film pressure is shifted to the exit of the oil in dynamic cases.
6. Under the effect of external harmonic forced vibration only, the maximum oil film pressure is higher as compared with the self-exited case by (51.92 %) for the same specifications of both journal bearing and oil.
7. The maximum oil film pressure is higher in the case of external harmonic forced vibration only as compared with the combined case by (24.1 %) for the same specifications of both journal bearing and oil.
8. Hence in case of external forced vibration only, the maximum oil film pressure is higher than that for both self-exited vibration and the combined effect for the same specification for journal and the oil but maximum oil film pressure dose not reach to the value of

heavily loaded journal bearing (2GPa.) to take the elastohydrodynamics effect into consideration.

6.2 Recommendations for future work

The following recommendation can be done for future work:

1. Other types of forced vibration source such as base excitation, whirling of shafts and rotating unbalance, can be studied on the journal bearing.
2. Finite length can be considered in z, x directions and study the effect of forced vibration on the performance of journal bearing.
3. Transient vibration effect on the performance of journal bearing can be studied.
4. Experimental work may be done in dynamic condition to verify both the numerical and theoretical results.

REFERENCES

1. **Uğur YÜCEL**, "Calculation of Dynamic Coefficient for Fluid Film Journal Bearings", Journal of Engineering science, Vol 11, pp. 335-343, 2005.
2. **Paulo Flores, JC Pimenta Claro and Jorge Ambrósio**, "Journal Bearing Subjected to Dynamic Loads, The Analytical Mobility Method", Mechanica Experimental, Vol 13, pp. 115-127, 2006.
3. **A. Bouzidane, M. Thomas**, " An electrorheological hydrostatic journal bearing for controlling rotor vibration", Computers and Structures, Vol 86, pp. 463-472, 2008.
4. **N B Naduvinamani, P S Hiremath and G Gurubasavaraj**, "Static and dynamic behavior of squeeze-film lubrication of narrow porous journal bearings with coupled stress fluid", Proc Instn Mech Engrs, Vol 215, Part J, 2000.
5. **M. Senthil Kumar, P.R. Thyla and E. Anbarasu**, "Numerical analysis of hydrodynamic journal bearing under transient dynamic conditions", Mechanica, Vol 82, pp. 37-42, 2010.
6. **K.V. Avramov, O. Borysiuk**, " Self-sustained vibrations of one disk rotor in two arbitrary length bearings", Mechanism and Machine Theory, Vol 70, pp. 474-486, 2013.
7. **Thomas Wirsing**, "Effect of Axial Oscillation on Performance of Hydrodynamic Journal Bearing", Cleveland State University, 2008.
8. **M. Lahmar, A. Haddad, D. Nicolas**, " An Optimized short bearing theory for nonlinear dynamic analysis of turbulent journal bearings", Eur. J. Mech, Vol 19, pp. 151-177, 2000
9. **Omidreza Ebrat, Zissimos P. Mourelatos, Nickolas Vlahopoulos, Kumar Vaidyanathan**, " Calculation of Journal bearing dynamic

characteristics including journal misalignment and bearing structural deformation", Tribology Transactions, Vol 47, pp 94-102, 2004.

10. N. K. Rana, S. S. Gautam and S. Samanta, " Approximate Analysis of Dynamic Characteristics of Short Journal Bearings in Turbulent Micropolar Lubrication", J. Inst. Eng. India Ser. C Vol 95, pp. 383-388, 2014.

11. Gwidon W. Stachowiak and Andrew W. Batchelor, "Engineering Tribology", 2'nd , Utter worth Einemann, Australia.

12. Singiresu S. Rao, "Mechanical Vibrations", 2'nd, Addison- Wesley Publishing Company, 2000.

13. Bernard J. Hamrock, "Fundamentals of Fluid Film Lubrication", NASA Reference Publication,1991

14. Bharat Bhushan, Principles and Applications of Tribology, The Ohio State University, Columbus, Ohio, 2013.

15. M. M. Khonsari and E. R. Booser, "Applied Tribology", 2'nd, John Wiley and Sons, Ltd. , 2008.

16. Basim Raheim," An Investigation in to Thermal Behavior of highly Loaded Bearings", University of Babylon, 2006.

APPENDICES

Appendix – A

The rigidity of the shaft is calculated for the center position of the disc and by using the integration method

$$EI \frac{d^2y}{dx^2} = M_{xx}$$

Where

E the modulus elasticity of the shaft material in N/mm^2

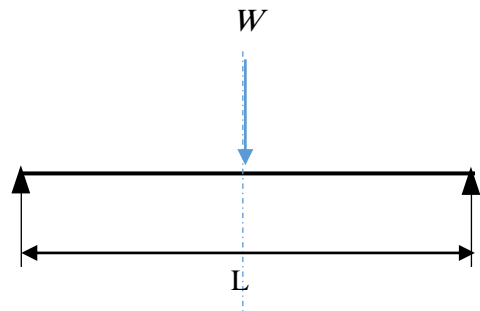
I the geometrical moment of inertia in mm^4 ($I = \frac{\pi d^4}{64}$)

d the diameter of the shaft in mm

$$EI \frac{d^2y}{dx^2} = \frac{w}{2}x - w\left(x - \frac{L}{2}\right)$$

$$EI \frac{dy}{dx} = \frac{wx^2}{4} - \frac{w}{2}\left(x - \frac{L}{2}\right)^2 + C_1$$

$$EIy = \frac{wx^3}{12} - \frac{w}{6}\left(x - \frac{L}{2}\right)^3 + C_1x + C_2$$



Applying the boundary condition

$$\text{At } x = 0 \quad y = 0 \quad \longrightarrow \quad C_2 = 0$$

$$x = L \quad y = 0 \quad \longrightarrow \quad C_1 = \frac{-3wL^2}{48}$$

Obtained

$$y = \frac{1}{EI} \left[\frac{wx^3}{12} - \frac{w}{6} \left(x - \frac{L}{2} \right)^3 - \frac{3wL^2x}{48} \right]$$

$$\text{At } x = 0 \quad y = \delta$$

$$\delta = \frac{1}{EI} \left[\frac{wL^3}{96} - \frac{3wL^3}{96} \right]$$

$$\delta = \frac{-wL^3}{48EI}$$

Where

δ the deflection of the shaft

The rigidity of the shaft is then can calculated as

$$k = \frac{w}{\delta}$$

$$k = \frac{48EI}{L^3}$$



Then

$$\omega_n = \sqrt{\frac{48EI}{mL^3}}$$

Appendix- B

B.1 The temperature meter and thermocouple

B.2 Oil specifications

Customer			
Name:	وزارة التعليم العالي والبحث العلمي / جامعة كربلاء / كلية الهندسة		
Address:	العراق		
Item under calibration			
Description:	TEMPERATURE RECORDER + TC (K)		
Manufacturer:	---		
Model:	---		
Serial number:	2		
Other identification:	(0 ----- 100) °C		
Date of reception:	28/04/2016		
Condition of reception:	GOOD		
Standard(s) used in the calibration			
Description:	Thermometer readout	PT100	Water bath
Manufacturer:	Fluke / USA	Fluke / USA	Hetogfrig / Danmark
Model:	1529	5615	---
Serial number:	B2C801	10860	---
Other identification:	---	---	---
Calibration information			
Date of calibration:	09/05/2016		
Place of calibration:	Temperature measurement lab		
Method(s) of calibration:	Calibration method using Working Thermometer - Calibration Procedure 2008		
Calibrated quantity:	Temperature / Celcius / °C		
Results of calibration:	Attached a complete result in Annex 1 of this certificate		
Measurement uncertainty:	There ported expanded uncertainty is based on GUM Standard and the standard Uncertainty multiplied by coverage factor k=2 to give confidence level of 95%		
Metrological traceability:	The traceability of measurement results to the SI units is assured by the National standard maintained at :- Central Organization for standardization and Quality Control through calibration at :- - COSQC/ Electrical lab (Cert. 028/2016/E) - Temp. measurement lab. (Cert. PH - 01-124-00) - NVLAB (REPORT NO. B3114057)		
Environmental conditions of calibration:	Temp. (25 °C);	±1°C	R. H.(50%) ±5%
Observations, opinions or recommendations:			
Performed by :	 MUSTAFA + NEDAL 10/05/2016		
	 1 of 1 Lamya I.M.Saad Ayoub 10/05/2016		
This certificate is issued in accordance with the laboratory accreditation requirements. It provides traceability of measurement to recognized national standards, and to the units of measurement realized at the COSQC or other recognized national standards laboratories. This certificate may not be reproduced other than in full by photographic process. This certificate refers only to the particular item submitted for calibration			

Calibration Certificate

Central Organization for Standardization and Quality
Control (COSQC)
Metrology Department

P.O. Box13032,Algeria street, Baghdad, Tel:7765180

E-Mail : cosqc@yahoo.com

Certificate No.: PF

406 / 2016

Date of issue :

09/05/2016

Results

Set Value C°	Reference Value C°	Indicate Value C°	Correction C°	ERROR C°	Uncertainty
25	25.6142	26.6	-0.9858	0.9858	0.610482103
50	50.6868	51.2	-0.5132	0.5132	0.613647664
80	81.0452	80.4	0.6452	-0.6452	0.625897796



Performed by:
MUSTAFA + NEDAL



Revised by:
JAMAL



Approved by:

Lamiya L.M. Saad Ayoub

2 of 1

This certificate is issued in accordance with the laboratory accreditation requirements, and to the units of measurement realized at the COSQC or other recognized national standards laboratories. This certificate may not be reproduced other than in full by photographic process. This certificate refers only to the particular item submitted for calibration.



Calibration Certificate

Central Organization for Standardization and Quality
Control (COSQC)
Metrology Department

P.O. Box13032 Algeria street, Baghdad ,Tel:7765180

E-Mail : cosqc@yahoo.com

Certificate No.: PF

404 / 2016

Date of issue :

09/05/2016

Results

Set Value C°	Reference Value C°	Indicate Value C°	Correction C°	ERROR C°	Uncertainty
25	25.6142	27	-1.3858	1.3858	0.610482103
50	50.6868	51.8	-1.1132	1.1132	0.613647664
80	81.0452	81.7	-0.6548	0.6548	0.625897796

Performed by:
MUSTAFA + NEDAL

Revised by:
JAMAL

Approved by:
Lanya I.M.Saad Ayoub

2 of 1

This certificate is issued in accordance with the laboratory accreditation requirements. It provides traceability of measurement to recognized national standards, and to the units of measurement realized at the COSQC or other recognized national standards laboratories. This certificate may not be reproduced other than in full by photographic process. This certificate refers only to the particular item submitted for calibration.



Figure (B.1): The calibration of temperature meter and thermocouples.

DAURA REFINERY
LABORATORIES DEPARTMENT
LUBE UNIT REPORT

OM & BLENDING: F.P. DATE: 5/7/15

PRODUCT: S3 Diesel Oils (155)

Batch No.	16F20		
Tank No.	60		
Is. Cst @ 40 C	198.21		
Is. Cst @ 100 C	18.80	On-SP	(15.5-21)
Viscosity @ 15.0 C	106	OK	95min
OC Flash C	246	On-SP	240 min
OC Fire C	266		
M. Flash T			
% Wt.			
Pour Point C	-12	On-SP	-9max
Water			
Phosphorus % Wt			
B. N. Mg KOH / gm Oil	13.5	On-SP	120min
Ap. Nu. Mg KOH / gm Oil			
Acid No. Mg KOH / gm Oil			
F. No. Sec.			
Sam. Res. % Wt			
Ash % Wt	(18922.B + HG11)		
Oil Ash % Wt	1.52	On-SP	(1.35-1.65)
TD. % Vol.	Nil	OK	Nil
Distillation % Vol.			
Imp. % Wt.			
Cast Test			
Dielectric Str. (2.5mm) K. V.			
Unken Lead Ib.			
foam @ 24 C	Nil	On-SP	Nil
foam @ 93.3 C	Nil	Stability	Nil
foam @ 24 C	Nil		Nil
Air Release Minut			
solubles % Wt.			
Phenol Antioxidant Test			
a % Wt			
TD) p.p.m.			
corrosive sulfur			
Net Sample Received			
Net Reprinted			

SIGNED

Figure (B.2): Oil specifications

الخلاصة

يعتبر المحمل الزيتي جزءا هاما لمعظم الآلات الدوارة. يتم استخدامه لدعم الأحمال الشعاعية. وهو ضروري لمنع تلامس المعادن بين الجزء الثابت (المحمل) والجزء الدوار (العمود). يعاني المحمل الزيتي من دوامة النفط غير المرغوب فيها نتيجة لارتفاع الاهتزاز الذاتي والأحمال الدورية مما يؤدي الى انعدام استقراره.

في هذه الأطروحة، تم التحقيق في أداء المحمل الزيتي في حالة مستقرة وحالة التحميل الديناميكي تحت تأثير الاهتزاز الذاتي و التوافقي القسري. لهذا الغرض، تم اعتماد المحمل الزيتي الهيدروديناميكية الاسطوانية.

تم تحليل الشكل التقليدي لمعادلة رينولدز تحليليا وعدديا باستخدام تقنية الاختلاف المركزي المحدود ضمن حدود أولية ومحددة وتم إجراء التحليل للمحمل الزيتي القصير.

تمت كتابة المعادلات العددية في برنامج الكمبيوتر (فورتران-٩٥) للحصول على النتائج.

وقد تم اختبار صلاحية جهاز المحمل الزيتي في مختبر الهندسة الميكانيكية في جامعة كربلاء لدراسة توزيع الضغط وقد تم مقارنة النتائج التي تم الحصول عليها مع النتائج العددية ووجدت أن هناك تباين كبير. لذلك تم استبعاد مقارنة النتائج العملية مع نتائج التحميل الديناميكية.

وفقا للنتائج العددية التي تم الحصول عليها، تم الحصول على أقصى ضغط لزيت تحت التأثير الثنائي لكل من الاهتزاز التوافقي القسري والذاتي هو (١٤.٨٧٧٨ ميجا باسكال) الذي ارتفع بنسبة (٣٦.٦٦) في المئة من تلك التي تم الحصول عليها تحت تأثير الاهتزاز الذاتي فقط. وكانت هذه القيمة تتزايد بشكل واضح مع زيادة اتساع الاهتزاز مما يسبب تذبذب كبير جدا والذي يؤدي إلى حدوث الفشل.

وقد وجد أن القيمة القصوى لضغط الزيت والقيمة الأدنى لسلك طبقة الزيت تأثرت بشكل واضح تحت تأثير الإثارة التوافقية القسرية بنسب التكرار والتخميد

أما بالنسبة لنسبة التردد ($\omega/\omega_n < 1$) فقد وجد أن الحد الأقصى للضغط يؤدي إلى انخفاض في الحد الأدنى لسلك طبقة الزيت، في حين أن الحد الأقصى لضغط الفيلم ينخفض بنسب التردد ($\omega/\omega_n > 1$) ، مما يجعل الحد الأدنى لسلك الفيلم يزداد ويؤدي الى تلافى الاتصال المعدني.

كما وجد أن نسبة التخميد العالية تسبب انخفاضا في اتساع الاهتزاز وهذا يؤدي إلى تقليل الضغط الأقصى لطبقة الزيت وبالتالي زيادة في سماكة طبقة الزيت. لنسب التخميد أعلى من ٠.٥ ، هناك تأثير قليل على الحد الأدنى لسمك طبقة الزيت.

ولوحظ أن قيمة الضغط الأقصى للزيت أعلى تحت تأثير الإهتزاز القسري الخارجي التوافقي فقط من قيمتها بتأثر الاهتزاز الذاتي فقط ، وتحت التأثير المشترك بنسبة (٢٤،١ ، ٥١،٩٢) في المئة على التوالي لنفس مواصفات المحمل والزيت . ومع ذلك، فإن أقصى قيمة لضغط فيلم طبقة الزيت لا تصل إلى قيمة (٢ كيكاسكال) ليأخذ بنظر الاعتبار التأثير الاستوهيدروديناميكية.



جمهورية العراق
وزارة التعليم العالي والبحث العلمي
جامعة كربلاء - كلية الهندسة
قسم الهندسة الميكانيكية

تأثير الأهتزاز على توزيع الضغط داخل المحمل الزيتي

رسالة مقدمة الى كلية الهندسة - جامعة كربلاء كجزء من متطلبات نيل درجة ماجستير علوم
في الهندسة الميكانيكية - ميكانيك تطبيقي

من قبل

هدى مسير عبد الكاظم

بكالوريوس ٢٠١٤

بإشراف

الاستاذ المساعد الدكتور عبد الكريم عبد الرزاق الحمداني